Review Article   **Open Access**

Zhiguang Zhou*, Enas Sakr, Yubo Sun, and Peter Bermel

Solar thermophotovoltaics: reshaping the solar spectrum

Abstract: Recently, there has been increasing interest in utilizing solar thermophotovoltaics (STPV) to convert sunlight into electricity, given their potential to exceed the Shockley–Queisser limit. Encouragingly, there have also been several recent demonstrations of improved system-level efficiency as high as 6.2%. In this work, we review prior work in the field, with particular emphasis on the role of several key principles in their experimental operation, performance, and reliability. In particular, for the problem of designing selective solar absorbers, we consider the trade-off between solar absorption and thermal losses, particularly radiative and convective mechanisms. For the selective thermal emitters, we consider the trade-off between emission at critical wavelengths and parasitic losses. Then for the thermophotovoltaic (TPV) diodes, we consider the trade-off between increasing the potential short-circuit current, and maintaining a reasonable open-circuit voltage. This treatment parallels the historic development of the field, but also connects early insights with recent developments in adjacent fields. With these various components connecting in multiple ways, a system-level end-to-end modeling approach is necessary for a comprehensive understanding and appropriate improvement of STPV systems. This approach will ultimately allow researchers to design STPV systems capable of exceeding recently demonstrated efficiency values.

Keywords: solar power, thermophotovoltaics, selective solar absorbers, selective emitters, selective filters

1 Introduction

Solar thermophotovoltaic (STPV) systems convert sunlight into electricity by absorbing solar photons as heat, which are then emitted as thermal radiation, which is subsequently converted into electron-hole pairs via a low-band gap photovoltaic (PV) medium; these electron-hole pairs are then conducted to the leads to produce a current [1–4]. Originally proposed by Richard Swanson to incorporate a blackbody emitter with a silicon PV diode [5], the basic system operation is shown in Figure 1. However, there is potential for substantial loss at each step of the process, particularly in the conversion of heat to electricity. This is because according to Wien's law, blackbody emission peaks at wavelengths of 3000 $\frac{\mu m \cdot K}{T}$, for example, at 3 µm at 1000 K. Matched against a PV diode with a band edge wavelength $\lambda_g < 2$ µm, the majority of thermal photons have too little energy to be harvested, and thus act like parasitic losses. This phenomenon often reduces STPV system efficiencies well below those of their PV brethren. If efficiencies could be substantially improved, new applications such as solar power with integrated storage would open up.
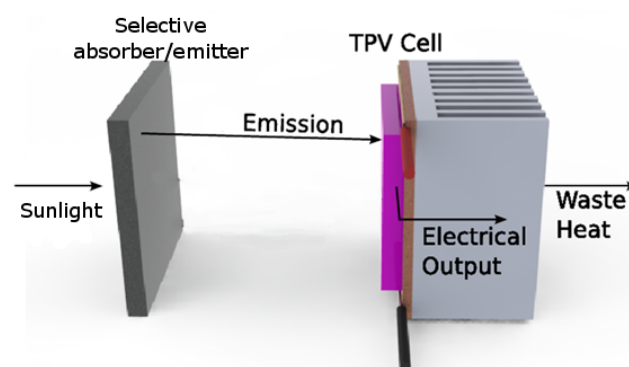

Fig. 1. Illustration of the basic design of solar thermophotovoltaic systems for converting sunlight into electricity. The efficiency may be limited by reradiation from the selective absorber, nonideal emission from the selective emitter and losses in the PV cell [3].

In accordance with the modular design of a STPV system, such as the one shown in Figure 2 [6], the system conversion efficiency can be broken down as a product of three component efficiencies [7]:

$$\eta_{STPV} = \eta_o \eta_t \eta_{tpv} \tag{1}$$

*Corresponding Author: Zhiguang Zhou: Birck Nanotechnology Center, Purdue University, 1205 W. State St., West Lafayette, IN 47907, USA, E-mail: zhou387@purdue.edu
Enas Sakr, Yubo Sun, Peter Bermel: Birck Nanotechnology Center, Purdue University, 1205 W. State St., West Lafayette, IN 47907, USA
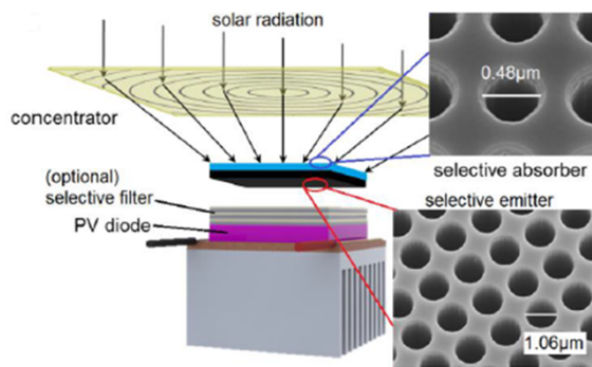
Fig. 2. Schematic of a photonic crystal-based selective solar absorber-selective emitter photovoltaic system (inset) scanning electron microscope picture of the 2D photonic crystal fabricated by Rinnerbauer et al. Reproduced with permission from [6]. © 2014 WILEY-VCH Verlag GmbH & Co. KGaA, Weinheim. All rights reserved.

where η_o is the concentration efficiency, governed by the concentrating optics, η_t is the thermal transfer efficiency of light into usable heat [8] and η_{tpv} is the TPV efficiency of converting heat to electricity. However, it is important to note that these three nominally independent terms still interact within the same system, and thus have many linkages, such as temperature, energy flux, and environmental conditions.

The initial theoretical development and improvement of STPV proceeded over the course of several years. Using Richard Swanson's concept as a baseline [5], the first key strategy for improving the system was to use a lower band gap PV cell than crystalline–silicon (c-Si). It was predicted that up to 65% efficiency would be possible with the use of a semiconductor having a band gap of 0.8 eV [9], which is about twice the Shockley–Queisser limit for a single-junction PV cell [10]. The primary reason is that many more thermal photons could be harvested with a lower band gap, which greatly reduces sub-band gap losses. The next key insight is to develop selective emitters that offer substantially different emission profiles than a black-body [9, 11, 12]. It could be seen early on that creating a selective thermal emitter that only emits thermal photons at or above the energy of the PV diode could wholly eliminate sub-band gap losses, although it would be a difficult goal. Experimentally, selective emitter materials such as rare-earth oxides (e.g., erbium oxide and ytterbium oxide [13]), as well as dielectric coatings on refractory metals (e.g., tungsten [W]) were shown to have potential for enhanced selectivity [14]. The third key insight was to introduce selective filters, in which a real selective emitter with less-than-perfect selectivity could have sub-band gap photons

returned to the emitter whence they came [4, 14, 15]. Subsequent calculations pointed toward experiments combining all three innovations [16]. On the strength of these results, it was subsequently re-estimated that in fact, STPV systems could in principle approach 85% conversion of sunlight to electricity under maximal concentration [17], a conclusion also reinforced by more recent work [18].

Developing integrated STPV systems to achieve even a fraction of the projected performance required significant advances in fabrication and characterization. A particularly key development was the adoption of a high-performance, low-band gap PV cell, made from Zn-diffused gallium antimonide (GaSb) in the late 1980s and early 1990s [19, 20]. Another key development in 1994 allowed STPV systems to reach sustained temperatures up to 1350°C [21]. Reliable operation for hundreds of hours over 1200°C, with up to 29% conversion of selected thermal emission to electricity was achieved shortly thereafter [22]. Within a decade, it was shown that the key underlying process of heat-to-electricity conversion could exceed 23% efficiency in experiment [23].

In recent years, there has been a competition to fully integrate and quantify the effects of using sunlight as the exclusive source of heat, and to improve overall STPV conversion efficiencies toward theoretical limits. Early system-level STPV results from Tohoku University in Japan [24] and Technical University of Madrid in Spain [25] reported experimental efficiencies below 1%. However, by 2013, an MIT group had achieved 3.2% efficient conversion [7]. Most recently, a collaboration out of Virginia and Argonne National Laboratories achieved 6.2% efficiency [26], although the test was performed with a 300 W laser diode source in lieu of direct solar simulation.

2 Principles of selectivity

Previous work has not addressed the problem of how to achieve much higher efficiencies, particularly those above the Shockley–Queisser limit of 31% [10]; the key problem has been a requirement for unrealistic alignment of emitter and receiver. Careful modeling of such designs suggests that it may be possible to strongly concentrate thermal emission into a much narrower range of photon energies. In fact, an integrated strategy could eliminate a separate filter, while achieving higher performance. This approach gives rise to a new type of thermal conversion known as thermophotonics [27]. This term indicates that emitted photons will always have energy above a nontrivial band gap value. Thus, the thermal emitter would end

up with a spectrum not unlike that of a light-emitting diode (LED), but with extraordinarily high efficiencies, since many of the typically loss mechanisms of LEDs would no longer be a problem with a thermal energy source. If typical sub-band gap and carrier thermalization losses due to above-band gap absorption can be strongly suppressed or even eliminated with this approach, extremely high heat-to-electricity power conversion efficiencies up to 50% could be achieved [28], well in excess of both the single-junction and tandem-junction Shockley–Queisser limits for PV cells [10]. This would be possible at 1300°C for band gaps ranging from 0.7 to 1.1 eV, encompassing a wide range of PV materials including GaSb and c-Si [29].

3 Selective solar absorber

The first step of STPV energy conversion is converting solar radiation into thermal energy by a solar absorber. In this section, we first focus on this step of the energy conversion. A main challenge is making a solar absorber that can both absorb broadband solar radiation and suppress re-radiation at high temperature. This challenge can be analytically expressed by the following figure of merit, called the thermal transfer efficiency [8]:

$$\eta_t(T_a) = \bar{\alpha}_a(T_a) - \frac{\sigma \bar{\epsilon}_a(T_a) T_a^4}{C I_{\text{solar}}} \qquad (2)$$

where $\bar{\alpha}_a(T)$ is the spectrally averaged absorptance of the solar absorber at temperature T_a, $\bar{\epsilon}_a(T)$ is the spectrally averaged emittance of the solar absorber, σ is the Stefan–Boltzmann constant, C is the concentration factor of the solar irradiance, and I_{solar} is the incident solar intensity that includes the loss during concentration.

Previous work used near-blackbody absorbers [30] like array of multi-walled carbon nanotubes [7] has very strong absorptance over a broad spectral range. However, their nonselective absorption also allows re-radiation over infrared (IR) wavelengths at high temperatures. Therefore, a selective solar absorber that has strong absorptance around the peak of AM 1.5 spectrum, yet weak absorptance at longer wavelengths, is preferred for high-performance STPV.

There are several types of selective solar absorbers that are suitable for STPV applications, including metal-dielectric composites, semiconductor–metal tandems, plasmonic absorbers, and one-dimensional (1D)/two-dimensional (2D)/three-dimensional (3D) photonic crystals (PhCs). Among the listed selective absorbers, metal-dielectric composites and semiconductor–metal tandems have similar thermal conversion efficiencies at tempera-

tures higher than 700 K [8, 31]. One-dimensional aperiodic multilayer PhCs follow closely behind, but have more complex structures [32]. For plasmonic absorbers and 2D or 3D PhCs, the slightly higher thermal emittance decreases their thermal transfer efficiencies at high temperatures. It is also relatively more challenging to fabricate plasmonic absorbers and 2D or 3D PhCs that are durable for high temperature operations [33, 34]. Other types of selective solar absorbers that have been previously considered in the literature, but are not explored here in detail, include textured absorbers [35–38] and intrinsic absorber materials [36, 38–40].

3.1 Metal-dielectric composite selective solar absorbers

Metal-dielectric composite solar absorber typically consists of cermet layers deposited on metallic substrates. A cermet consists of nanoscale metal particles embedded within ceramic binders [30]. Typical ceramic binder materials include alumina (Al_2O_3) [41], silicon dioxide (SiO_2), aluminum oxynitride (AlON) [8] and zirconium dioxide (ZrO_2) [42]. The cermet layer by itself has strong solar absorption and high transmission in the mid-IR. Combined with a metallic substrate, which is highly reflective at mid- and far-IR, the cermet offers both strong solar absorption and low thermal emittance. The cutoff of strong absorption and scattering in cermet can be tuned by the sizes of the metal particles. For example, larger particle sizes correspond to longer cutoff wavelengths [43]. The thickness of the cermet layer also needs to be carefully engineered. Thicker cermets lead to stronger solar and IR absorption [43]. Previously, a graded concentration of metal particles was proposed to improve solar absorption within the cermet by gradually increasing the refractive index of each cermet layer [30]. A single layer of graded Ni/Al_2O_3 on stainless steel was reported to have an averaged solar absorptance of 94%, and an averaged thermal emittance of only 7% at 773 K [31]. It is also proposed that for Al^{sp}-AlON (Al sputtered in AlON binder) cermet solar absorber, a ten-layer graded cermet can be simplified as a double-layer cermet, yielding 86% thermal transfer efficiency at 1 sun illumination and a temperature of 353 K [8]. Another type of cermet structure uses porous alumina as the ceramic binder. The pores are perpendicular to the metallic substrate and can be filled with nanoscale metal [nickel (Ni), vanadium (V), cobalt (Co), copper (Cu), chromium (Cr), molybdenum (Mo), silver (Ag), tungsten (W)] rods [44]. Finally, as shown in the simulated reflection spectra in Figure 3B, using W particles in an alumina binder multilayer

structure (Figure 3A) is predicted to achieve up to $\eta_t = 86\%$ under 100 suns at 1000 K [45].
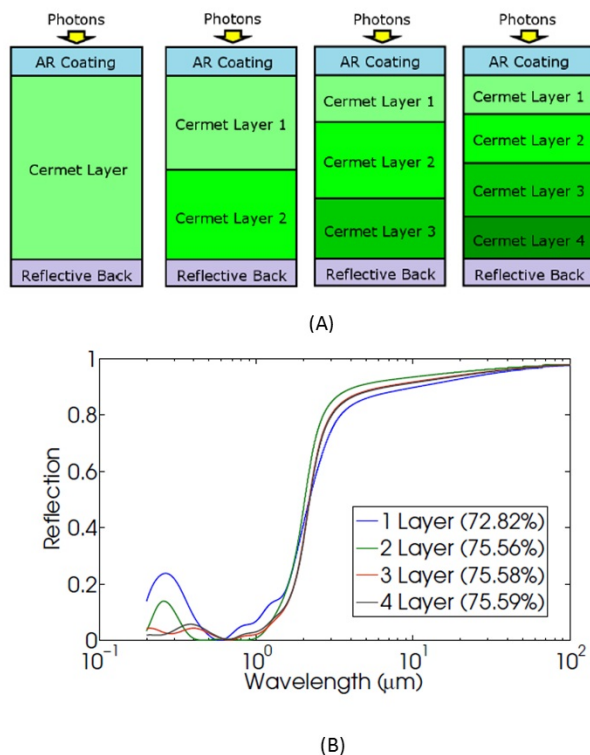

(A)

(B)

Fig. 3. Cermet selective solar absorber. (A) Schematic drawing of the cross-section of multilayer W cermets. (B) Simulated reflection spectra of optimized multilayer W cermets. Panels (A) and (B) adapted with permission from [45]. © 2011 Optical Society of America.

3.2 Semiconductor–metal tandem selective solar absorbers

Another type of selective solar absorbers uses the spectral selectivity of semiconductors. Low-to-medium band gap semiconductors (0.5–1.26 eV), like crystalline silicon (c-Si), amorphous silicon (a-Si) [46], germanium (Ge) and lead sulfide (PbS) [47–49], have strong solar absorption. Furthermore, when intrinsic or lightly doped, and polished, they can be almost transparent to photons with energy below their band gaps. By using metals with low thermal emittance as back reflectors, a semiconductor–metal tandem absorber may exhibit both strong solar absorption and low thermal emission. To reduce the reflection of the solar incidence due to the high refractive index of the semiconductors, an anti-reflection layer can be coated on top of

the semiconductor. It is recently proposed that a multilayer front coating consisting of four gradually increasing index materials (Figure 4A) can significantly improve the absorptance and selectivity of the Ge + Ag semiconductor–metal tandem absorber as shown by the simulated emissivity spectra in Figure 4B, yielding an 88.1% thermal transfer efficiency at 1 sun illumination and a temperature of 400 K [50]. For high temperature (1000 K) applications, Ge in the proposed absorber design was substituted with Si. Under 100 suns illumination, η_t reaches 82.2% [50].
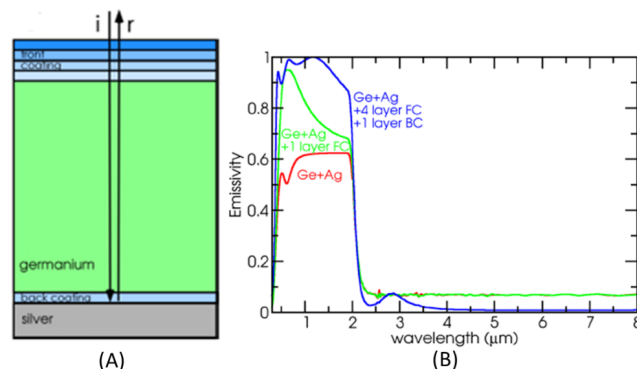

(A)　　　　　　　(B)

Fig. 4. Ge + Ag tandem selective solar absorber. (A) A schematic drawing of the optimized Ge + Ag tandem selective absorber with four front coating layers and a back coating of low index material. (B) Simulated emissivity spectrum showing that the front coating and back coating improve the overall emissivity before the cutoff wavelength while suppressing the parasitic emissions. Panels (A) and (B) adapted with permission from [50]. © 2010 Optical Society of America.

3.3 Plasmonic selective solar absorbers

Plasmonic nanostructures, made of highly conductive metals with strong surface plasmon resonances, may enhance absorption around selected incident wavelengths and angles. The resonant frequencies can also be tuned by the dimensions and material properties of the structure (using metal nanostructures and dielectric spacers). Therefore, plasmonics have been proposed as a relatively new type of selective solar absorber. A plasmonic absorber consisting of Ni nanochains embedded in Al_2O_3 was recently proposed, as shown in Figure 5A, which operates not entirely unlike a cermet. The surface plasmon polaritons resonance of Ni is broadened by the chain structure. The net result shown in Figure 5B shows that the solar absorptance is larger than 90% and the thermal emittance loss is <10% at 673 K [51]. This is equivalent to 92% solar thermal transfer efficiency at 673 K and 100 suns illumina-

tion. A 2D planar plasmonic integrated absorber/emitter was proposed to be able to function as both selective solar absorber and selective thermal emitter, as schematically shown in Figure 5C. As shown in the simulated spectra in Figure 5D, the visible absorption of the two enhanced absorption peaks are used to collect incident solar radiation, while the IR absorption is used for selective thermal emission [52]. Since this operation mode is distinct from more conventional selective solar absorbers, it is not meaningful to calculate a solar thermal efficiency here. It is also important for selective solar absorbers to survive under high operating temperature. Nanostructures are particularly prone to partially losing their structures upon heating, due to the small radius of curvature associated with sharp nanoscale features. A possible solution to this dilemma may be the strategy of using refractory plasmonics [53, 54].
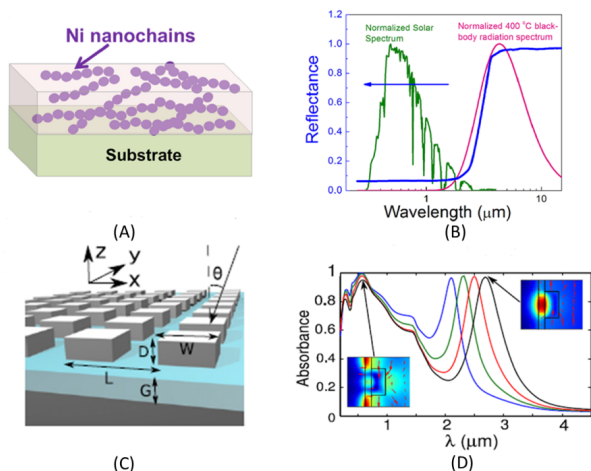

Fig. 5. Should be: Plasmonic selective solar absorbers. (A) A schematic drawing of the selective absorber with Ni nanochains embedded in Al_2O_3. (B) Reflectance spectrum of the selective absorber with Ni nanochains embedded in Al_2O_3 (blue line) shows high selectivity to avoid thermal reradiation when operating at a temperature of 673 K. Panels (A) and (B) adapted with permission from [51]. © 2012, AIP Publishing LLC. (C) Schematic drawing of the 2D planar plasmonic integrated absorber/emitter. (D) Simulated absorbance spectrum of the integrated absorber/emitter. High-energy absorption peak and low-energy absorption peak for solar irradiance absorption and thermal emission, respectively. The low-energy absorption peak can be tuned by the dimensions of the patterning feature. Peak from left to right corresponds to L = 383 nm; W = 206 nm; D = 83 nm; G = 27 nm/L = 393 nm; W = 230 nm; D = 79 nm; G = 24 nm/L = 404 nm; W = 252 nm; D = 73 nm; G = 23 nm/L = 396 nm; W = 269 nm; D = 72 nm; G = 22 nm. Panels (A) and (B) adapted with permission from [52]. © 2012 IOP Publishing. All rights reserved.

3.4 PhC selective solar absorbers

A PhC is another type of selective solar absorber. PhCs are characterized by a photonic band gap, a selected range of wavelengths that are strongly reflected. Combined with a suitable absorber, this can give rise to selective solar absorption. The absorption cutoff can be tuned by adjusting the dimensions of the periodic structure, and thus shifting the photonic band gap. Furthermore, PhCs can also enhance absorption via quality factor matching (Q-matching) [29, 50, 55, 56]. According to coupled mode theory [57], a cavity with a resonance frequency ω_0 and absorption quality factor Q_{abs}, and coupled to a radiating mode with a quality factor Q_{rad} has an absorption spectrum given by the following:

$$A(\omega) = \frac{4/(Q_{abs}Q_{rad})}{\left(\frac{(\omega - \omega_0)}{\omega_0}\right)^2 + \left(\frac{1}{Q_{abs}} + \frac{1}{Q_{rad}}\right)^2} \quad (3)$$

At resonance, maximum absorption can be obtained if Q_{abs} = Q_{rad}. A 1D multilayer stack [32] was recently proposed and a 1D V-shaped grating consisting of similar multilayer structures was simulated by the same research group [58]. For certain parameters, 2D PhC selective solar absorbers may also have wide angle selective absorption [59, 60]. This design was recently realized in experiment [6], as shown in Figure 6A. The optimized tantalum (Ta) PhC solar selective absorber can have a thermal transfer efficiency of 66.4% at 1000 K when illuminated by 100 suns [6]. Combining a 2D PhC and a 1D chirped multilayer, an integrated PhC may have extremely strong selectivity after optimization. High-quality 3D PhCs with strong selectivity have also been fabricated [61], as shown in Figure 6B, and can be potentially used as solar absorbers in STPV systems. For high temperature applications, the PhC structure should be made of refractory materials. In our recent work [29], it was suggested that W, Mo, tantalum (Ta) and Cr are the four refractory metals that are most practical for large-scale, high-performance applications.

Clearly, high operating temperatures are required for high-performance STPV systems. However, a strong overlap between the blackbody radiation and solar irradiance spectra at high temperatures makes it challenging to achieve both high spectrally averaged absorptance $\bar{\alpha}$ and low spectrally averaged emittance $\bar{\epsilon}$. One option is to increase the solar concentration, so that the impact of a larger $\bar{\alpha}$ can be alleviated. It has been demonstrated that a 2D Ta PhC with moderate selectivity has 82.8% thermal transfer efficiency under 1000 suns concentration at 1500 K [62]. However, 1000 suns concentration requires 2-axis precision tracking [63], adding more complexity to the
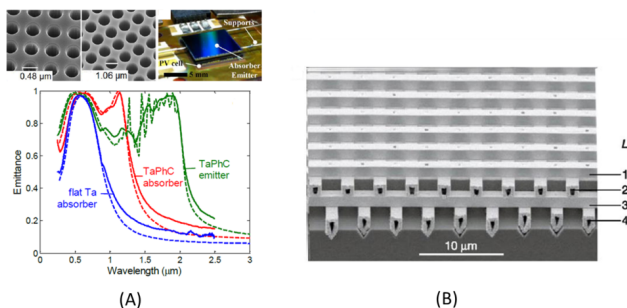
Fig. 6. PhC selective solar absorbers. (A) Two-dimensional PhC selective absorber and selective emitter and their measured emittance spectrum [6]. (B) Scanning electron microscope picture of the 3D PhC fabricated by Fleming et al. Adapted by permission from Macmillan Pulishers Ltd: Nature [61], © 2002.

STPV system. Another less investigated option is designing a highly selective solar absorber. The strong selectivity allows decent thermal transfer efficiency even under low solar concentrations ($\leqslant$100 suns). This option keeps the STPV system relatively simple. Therefore, the design and fabrication of highly selective solar absorber for high operating temperature and low solar concentration warrants further investigation.

4 Selective thermal emitters

Selective thermal emitters play a major role in enhancing STPV system efficiency. Without them, it is typically hard to reach efficiencies above a few percent. The reason is as follows: in comparison to conventional solar power PV systems, STPV systems convert concentrated sunlight into heat that is re-radiated by an emitter toward the PV cell. Since the emitter's temperature is typically well below the temperature of the sun (<5500 K), the vast majority of the thermal emission lies below the band gap of the PV converter. This implies that spectral shaping of emission is necessary to enhance the emission of high-energy photons above the PV band gap, while suppressing the emission of low-energy photons below the PV band gap.

Accordingly, there are some general design requirements for selective thermal emitters to efficiently harvest heat energy generated from concentrated solar radiation. Ideally, the selective thermal emitter should enhance the emission of photons with energies above the band gap of the PV diode, while completely suppressing sub-band gap photons. However, the restriction of the selective radiation band can be safely neglected. The reason is that the spectral radiance of an arbitrary emitter whose temperature is below 2500 K tends to fall off sharply for suf-

ficiently high-energy photons. This suggests that thermalization of energetic electrons due to above-band gap absorption is not a major loss mechanism in STPV, compared with solar PV. Consequently, the largest losses are contributed by sub-band gap photons that are not absorbed by the PV converter [28]. Another requirement is to have a sufficient emission bandwidth above the band gap to produce a sufficiently high open circuit voltage. In fact, there is an optimum nonzero emission bandwidth, for example, the optimum emission bandwidth for an emitter at 2000 K was found to be around 0.07 eV [28]. One final basic requirement for the selective emitter is to maintain mechanical and thermal stability under temperatures as high as 1500°C for long periods of time.

The above requirements can be satisfied using a variety of materials and structures. Rare-earth elements such as erbium, thulium, ytterbium, samarium, and holmium exhibit naturally selective emission with sufficiently high melting points [13, 64–66]. These qualities make them good candidates for selective emitters for TPV systems. Another class of materials that show high stability under high temperature operation is refractory metals, such as W, Ta or molybdenum [29]. However, refractory metals are known to have a wide emission spectrum and their respective TPV efficiency is low, unless spectral shaping is introduced. It may be achieved by using cold-side filters [67], modifying the photonic density of states to achieve wavelength selectivity, or combining emitter selectivity with a filter [29]. The 1D, 2D or 3D PhCs [50, 61, 68–70] and metamaterials [52, 54, 71] are good examples of structures that can strongly modify the photonic density of states. In fact, among all of these approaches, 2D metallic PhCs have garnered the greatest interest for STPV systems [6, 7, 68], because of the high abundance ranking of refractory metals, and the ability to preferentially tailor near-blackbody emissivity at the designed wavelength range and suppress emission outside. Indeed, high experimental efficiencies were obtained using integrated selective solar absorber-emitter 2D PhCs. For example, STPV efficiency of ~10% was proposed by Nam *et al.* [68] using 2D Ta PhC, and 3.74% at 1000 K experimental STPV efficiency was achieved by Rinnerbauer *et al.* [6]. A simpler, scalable and compact STPV system based on 1D Si/SiO$_2$ PhCs has also been proposed with experimental efficiency of 3.2% [7]. Another potential candidate for selective emitters is recently suggested using titanium nitride, as a refractory plasmonic material that can maintain structural stability at temperatures as high as 833 K [54].

4.1 Rare-earth emitters

Rare-earth-based selective emitters were among the first materials considered for this application [13]. As was previously mentioned, rare-earth-based emitters have naturally selective emission that can be matched to available PV cell technologies. For instance, erbium oxide and ytterbium oxide can be fabricated either in a mantle structure [65], coated on a foam ceramic [67] or on $MoSi_2$ substrates [72], and can be used as thermal emitters whose selective radiation band matches well with Si and Ge PV cell band gaps. Figure 7A shows the spectral matching between a mantle ytterbium(III) oxide (Yb_2O_3) emitter and Si PV cell. Rare-earth elements can also be doped into rigid host materials, such as yttrium aluminum garnets [64], or fused silica glass [73] and backed by a metallic reflector to prevent emission to the back side. Although rare-earth elements have their inherent natural selectivity, they still show low spectral efficiency, caused by either intrinsic emission tails of rare-earths at longer wavelengths, or by metallic back reflectors parasitic emission [64]. There is also a trade-off between narrow linewidth emission from rare-earth atom dopants versus rare-earth oxides with line broadening for greater overall thermal emission in bulk. Hence, incorporating rare earths into artificial structures could help fine-tune these characteristics, potentially enhancing their spectral efficiency. For example, recent work has shown that improved spectral and TPV system efficiencies for rare-earth-doped garnet emitters with GaSb PV cells can be achieved using the concept of quality factor matching [74]. Additional improvement is expected when the conventional metallic back reflector is replaced by a quarter-wave dielectric stack (QWS), and a chirped dielectric filter on top of the structure is integrated [74], as shown in Figure 7B and 7C. Metasurface back reflectors are also suggested for emission enhancement of optically thin rare-earth-doped glasses employing generalized Snell's law. The idea is to modify reflection angles upon multiple bounces on the reflecting metasurface and eventually couple to a surface mode to achieve complete absorption [73].

4.2 PhCs and metamaterial thermal emitters

As discussed previously, PhCs support a wide band gap that can be designed to suppress sub-band gap emission. An example of a Si/SiO_2 1D PhC is shown in Figure 8A and 8B. Resonant emission in metallic 2D PhCs can be engineered to enhance useful emission via Q-matching [56]. An array of a W 2D PhC and the tailored thermal emis-
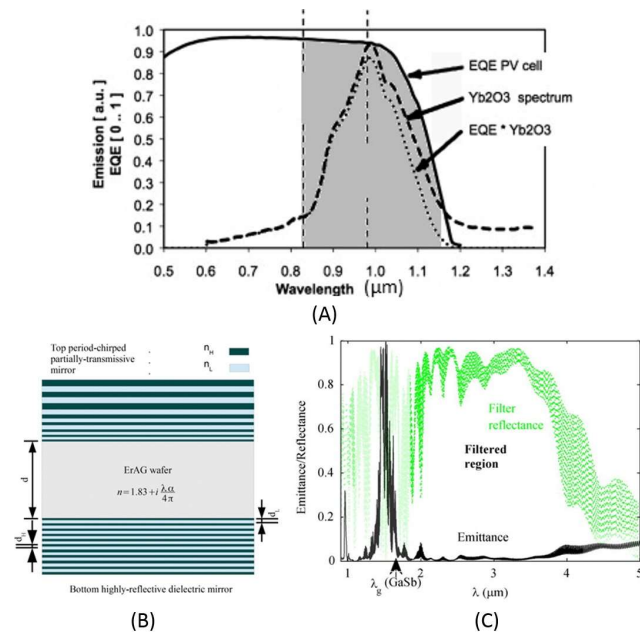

Fig. 7. Rare-earth emitters. (A) Yb_2O_3 emission and the external quantum efficiency (EQE) spectrum of Si PV cell. The convolution with the Yb_2O_3 spectrum is shown between 0.6 and 1.4 μm wavelength [67]. (B) A schematic of the high efficiency rare-earth emitter proposed in with chirped-mirror. The bottom dielectric mirror is a QWS with reflection centered at 1.47 μm. The top dielectric mirror has an exponentially chirped period with up to 26 layers that reflects all the wavelengths from 2 to 4 μm. The ErAG wafer is assumed to be much thicker than the dielectric layers surrounding it. (C) The calculated spectral emittance of the structure is shown in (B). Panels (B) and (C) adapted with permission from [74]. © 2014, AIP Publishing LLC.

sion is shown in Figure 8C. Also, Kohiyama *et al.* proposed a closed-end surface microcavity array to improve the emission quality factor and hence suppress thermalization losses [75]. Three-dimensional PhCs are also proposed as efficient thermal emitters, either being an all-metallic structure, as first proposed in [61, 76], or with a metal-coated silicon or carbon scaffold for improved thermal stability [70, 77]. Figure 8E (inset) shows an example of a 3D metallo-dielectric structure and the measured selective emission at 889 K is shown in Figure 8E. On the other hand, there are a number of fabrication challenges associated specifically with multi-period 3D PhCs [78], which have encouraged the investigation of structures simpler to fabricate.

Metamaterials also can be optimized to support plasmonic resonances, which make them perfect absorbers in a given frequency range [71]; by Kirchhoff's law of thermal radiation [79], which also makes them perfect emitters. It is also possible to design wide-band emission spectrum by including different sub-cell elements in the unit cell of the
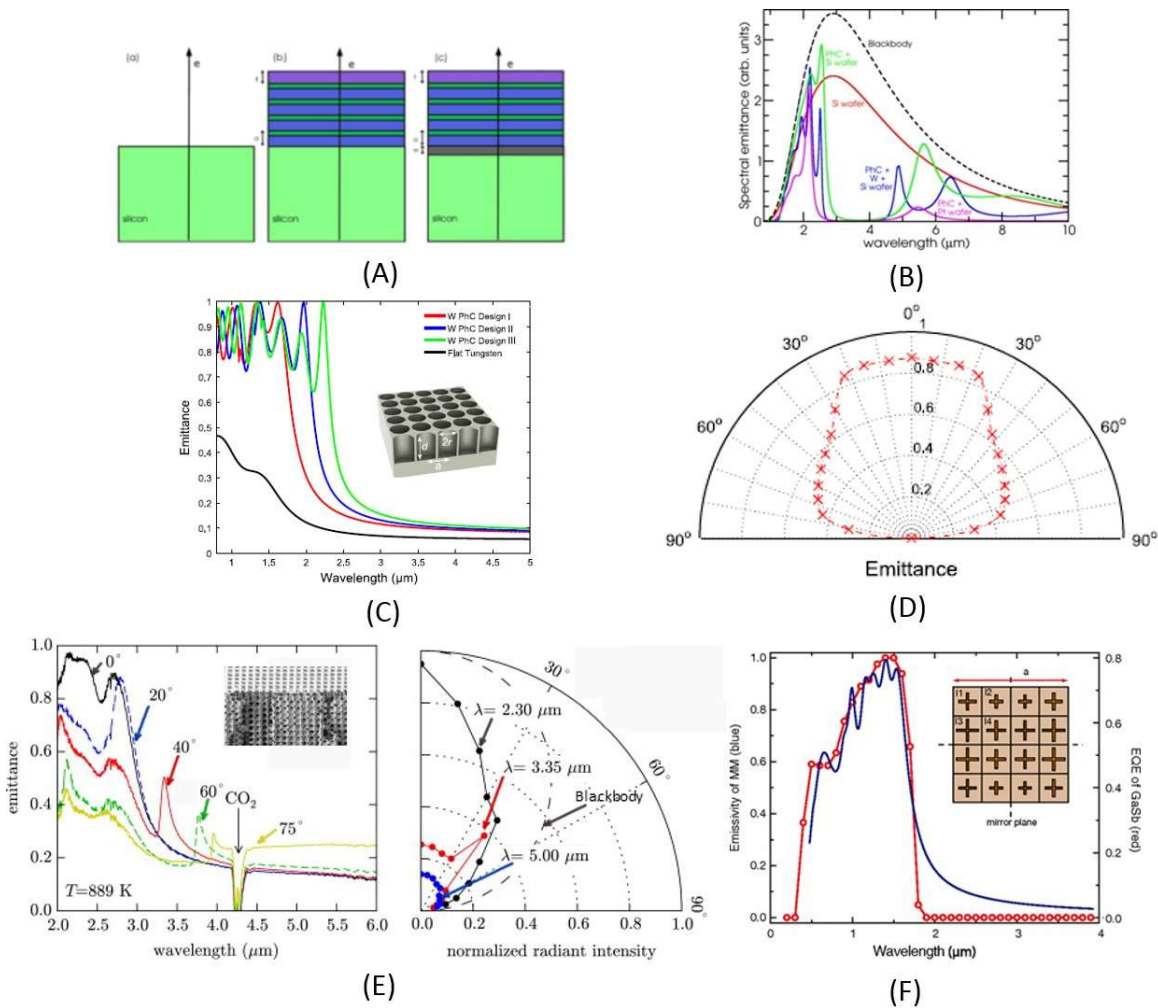
Fig. 8. Photonic crystal and metamaterial emitters. (A) Example of 1D Si/SiO_2 PhC, where an optimized number of layers exhibits the spectral emissivity shown in (B). Panels (A) and (B) adapted with permission from [50]. © 2010 Optical Society of America. (C) Simulated normal emittance for W PhC design I (r = 0.45 μm, a = 1.10 μm, d = 1.50 μm), W PhC design II (r = 0.55 μm, a = 1.30 μm, d = 2.10 μm), W PhC design III (r = 0.625 μm, a = 1.40 μm, d = 2.80 μm). Near blackbody performance below the cutoff wavelength is clear compared with flat W [55]. (D) A polar plot of the average emittance below the cutoff wavelength (i.e., $\lambda \leqslant 2$ μm) for W PhC design II [55]. (E) (inset) Scanning electron microscope image of the broken side of a 3D Si/Pt PhC [70]. The ALD Pt film covers the full 3D structure. (left) Spectral emittance measured for the 3D PhC at 890 K for different exit angles. (right) Normalized radiant intensity polar plot for several wavelengths. The dashed line represents the blackbody curve [70]. (F) Designed metamaterial with wide-band emissivity from [71] (blue curve) and EQE (red curve) of GaSb. Inset shows a schematic of the metamaterial design with 16 sublattices. Panel (F) adapted with permission from [71]. © 2011 The American Physical Society.

metamaterial structure, as shown in Figure 8F. Moreover, these types of emitters can also be integrated with selective solar absorbers [6, 68].

Numerical simulation of thermal emission from such complex electromagnetic structures is essential to understand and optimize their performance. The direct method of simulating thermal emission is based on the fluctuation-dissipation theorem [80]. The advantage of this method is that it captures the physical nature of thermal emission from fluctuating thermal currents, and models the emission, propagation and absorption of thermal radiation between bodies [81]. This makes fluctuation thermodynamics particularly important to study near-field thermal energy transfer that is the essence of near-field TPVs (NFT-PVs) [81–84].

In other cases, particularly in the far-field, the selective emission property of any structure of a given material can be readily predicted by Kirchhoff's law of thermal radiation [79], which simplifies the problem of simulating the random nature of thermal emission to that of designing a perfect absorber [85]. Indeed, this approach makes it easier to optimize the structure's geometry to obtain near-

blackbody emissivity at the desired PV conversion energy band using the Q-matching concept.

An example of employing the Q-matching concept on a simple 1D structure is the vertical-cavity enhanced resonant thermal emitter (VERTE) [86]. The concept of Q-matching can also be used to design a 2D W PhC [69], and Ta PhC [68, 87], through controlling the period, radius and depth of the PhC holes array to obtain maximum emissivity at the microcavity resonance [29, 56]. Example of 2D PhC emittance spectrum is shown in Figure 8C. A survey of the TPV performance for different refractory metals that could be used as 2D PhC thermal emitters is provided in [29]. The Q-matching concept is also used to enhance the emissivity of metamaterial emitters [52, 71].

4.3 Filters and photon recycling

Even with improved selective emitter designs, some parasitic emission generally remains in the mid- and far-IR [67]. This sub-band gap emission is expected to cause the greatest system efficiency losses [28]; thus, filtering becomes necessary to significantly improve the STPV efficiency and reuse the unabsorbed low-energy photons. As a result, this topic has drawn a great deal of interest for a number of years [14]. Ideally, a filter should transmit all the radiation above the band gap and reflect all sub-band gap emission. Such a requirement is hard to meet, but there are a number of structures that can provide a sufficiently wide reflection band in the IR region. Plasma filters based on transparent conducting oxides [88, 89] or semiconductors [90] with plasma frequency adjusted to the band gap of the PV cell were suggested as edge filters for TPV applications. An example of the reflection of an InN-based plasma filter is shown in Figure 9A. Another option is a dielectric 1D PhC, based on a QWS [4, 91]. Metal-dielectric 1D PhCs, with thin metallic layers, may provide even larger photonic band gaps [92]. An example of the structure of a 1D ten-layer Si/SiO$_2$ PhC and the corresponding reflectivity is shown in Figure 9B. Plasma filter can be combined with a QWS to suppress undesired emission at longer wavelengths [88]. Introducing chirping to the QWS period can also provide larger coverage of the stop-band. However, the aforementioned types of filters generally exhibit secondary lobes just outside the photonic band gap and harmonics at shorter wavelengths that results in reduced transmission over a wide range of the pass-band. An effective, but expensive, way to achieve near-perfect performance is to introduce continuous sinusoidal variation of the refractive index by including mixtures or alloys of the two end materials, known as a rugate filter [15, 93]. Al-though fabrication of an ideal rugate filter is challenging, an alternate method is to quantize the refractive index sinusoidal function into a finite set of piece-wise constant index materials [94]. Figure 9C shows four possible designs of the discretized rugate filter with six materials along with the corresponding equivalent index and stop-bands of the four designs, as proposed by Carniglia [94].

The advantage of these filters is not only to reduce parasitic emission, but also to recycle low energy photons by reflecting them back to the emitter [50]. Effective recycling of sub-band gap photons leads to a noticeable improvement in the TPV system efficiency.

Although the previously mentioned types of filters were originally designed to be placed at the cold side, which is just above the PV cell or as part of its back reflector [95], an integrated emitter-filter has recently been suggested for improved spectral efficiency of rare-earth emitters [74]. The concept can be applied to any type of selective emitters, including 2D PhCs, after filling their holes with a supportive dielectric for mechanical stability.

4.4 Near-field TPV

An inherent limitation of far-field TPV conversion is the low output power dictated by the blackbody limit. Thus, near-field power conversion is a potential strategy to enhance the output of TPV systems [81, 96]. In contrast with far-field TPV power conversion, bringing the emitter closer to the PV cell (nano- or microscale separation distances) allows tunneling of evanescent surface modes. These new channels of energy transfer could potentially enhance thermal emission and overcome the blackbody limit [84, 97, 98].

In fact, the increased radiative heat transfer between two metallic surfaces in proximity due to contribution of evanescent waves was measured in the late 1960s [99, 100]. In 1971, near-field heat transfer was theoretically explained by Polder and van Hove [101], based on the stochastic electrodynamics framework of Rytov *et al.* [80, 102, 103].

For TPV conversion, DiMatteo *et al.* [104] pioneered an early realization of micron-gap near-field thermal transfer between an InAs-based prototype PV diode and a silicon heater chip fabricated using microelectromechanical system technique to control the micron-gap separation between the heater and the PV diode. An observed fivefold increase in the short-circuit current was interpreted as an evanescent-coupling effect on the heat transfer. In 2005, DiMatteo *et al.* [105] provided a conclusive assessment of their proposed micron-gap TPV experimental setup by car-
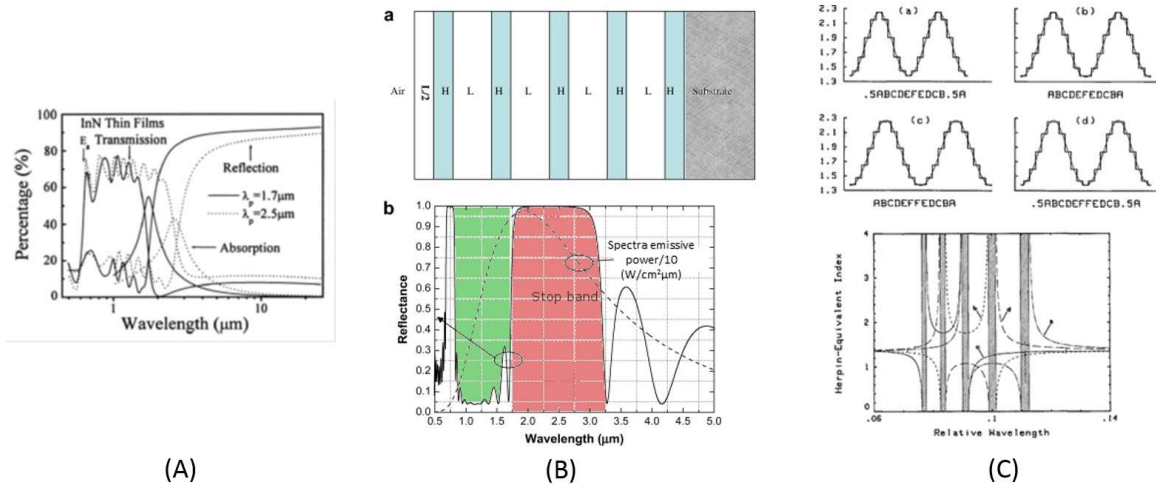
Fig. 9. Types of filters used in STPV systems. (A) The reflection of an InN-based plasma filter, the plasma wavelengths of 1.7 and 2.5 μm corresponding to the band gap of GaSb and GaInAsSb PV cells, respectively. Eg represents the band gap of InN. Panel (A) adapted with permission from [90]. © 2002, AIP Publishing LLC. (B) An example of a 1D ten-layer PhC (a), described as $L/2H(LH)^4$, where L and H represent quarter-wavelength thick layers of SiO2 (low refractive index) and Si (high refractive index), respectively, while L/2 represents half-quarter-wavelength thick layer of SiO$_2$ and the corresponding normal incident reflectance of 1D Si/SiO$_2$ $L/2H(LH)^4$ PhC and the spectra emissive power of a blackbody radiator at 1500 K (b). Adapted from Mao and Ye [91]. (C) (Top) Four ways of approximating a rugate filter by a stepped index design. The continuous curves correspond to an index profile in which the log of the index is sinusoidal. (Bottom) Herpin-equivalent (effective medium) index of the four six-material designs in the vicinity of the stopbands. The curves are labeled with letters corresponding to their representation in the top figure. The stopbands themselves are shaded. Panel (C) adapted with permission from [94]. © 1989 Optical Society of America.

rying out measurements at higher temperatures, increasing the area and current capacity of the PV diode array, and minimizing associated thermal conduction losses by using tubular spacers. They found the output power was highly dependent on the series resistance, shunt resistance and temperature of the PV diode, suggesting a need to redesign PV diodes for higher current capacities, as well as the need to develop thermal emitters and maintain high temperature difference under such small spacings with minimized heat conduction contribution. Similarly, Hanamura and Mori [106] measured the radiated power for nanoscale gaps for a contactless system of a GaSb cell and a W emitter. A remarkable increase in the output power was noticed at gaps <1 μm.

In fact, the design of a nanogap TPV system is affected by three kinds of losses that may dominate according to the specific system designs. These losses are radiative losses, electrical losses and thermal losses. Radiative losses are considered in different studies [96–98, 107], with the suggestion of using a graphene layer in the PV cell for better coupling [107]. Electrical losses in NFTPV systems were also studied thoroughly by Park et al. [108], with the conclusion that smaller gaps do not always lead to improved conversion efficiency; nevertheless, diffusion and recombination losses reduce the efficiency by 5–10% as predicted in their model, and decreases for vacuum gaps

<10 nm. For such small gaps, more radiation is absorbed near the surface, which creates increased surface recombination. The third kind of loss comes from increased PV diode temperatures, which suggests a need for effective PV thermal management [109]. The combined effect of the three kinds of losses has been studied by Bernardi et al. [84]. A unifying solution comes from spectral shaping of the radiator. In a related development, Molesky and Jacob [82] suggested introducing a matched van Hove singularity in the absorbing photocell-emitter pair to significantly improve efficiencies. Similarly, properly designed thin film emitters and receivers give rise to thermal analogs to quantum wells [110], known as 'thermal wells', which may improve power conversion efficiency. Finally, refractory hyperbolic metamaterials (HMM) [111] are good candidates for near-field thermal energy transfer. HMMs can be realized in either a multilayer structure of alternating subwavelength metallic and dielectric layers, or in a metallic nanowire structure embedded in a dielectric medium. The hyperbolic dispersion behavior exhibits enhancement of high momentum components that act as energy channels for evanescent modes. Access to these high momentum channels is the key to achieve super-Planckian heat transfer between bodies in near proximity.

NFTPV is a technically challenging yet theoretically promising approach to converting heat to electricity. With

all the ongoing research in this area, an optimum design of an efficient NFTPV can boost the efficiencies dramatically, although experimental investigation of the realization of NFTPV generators is still under study. Hence, efficient cooling strategies for the PV cell, as well as the capability to maintain precise alignment between emitters and receivers with small gaps, while minimizing conducting losses, and finding the optimum design of the PV converter are the main challenges of this technique.

4.5 Angular selectivity

In standard solar PV, the PV cell receives radiation directly from the sun, which can mostly be considered as a narrow-angle source with almost normal incidence on the cell. Conversely, in STPV, the PV cell receives radiation from an emitter that is close to its surface, thus the PV cell receives radiation from all angles. Consequently, the angular distribution of thermal emission is a nontrivial factor in determining the STPV efficiency [112]. Interestingly, the structure of the selective emitter has a big impact on the angular selectivity. A flat blackbody, for example, follows the Lambert's cosine law of radiation, thus uneven emission is attained from different angles, whereas angular emission can be tailored using more complex structures. For example, the VERTE structure described in [86] exhibits narrow angular thermal emission lobes for the corresponding defect resonant wavelengths. Two-dimensional PhCs also exhibit angular selectivity for normal incidence and a high emissivity is observed for all angles below the diffraction threshold, as shown in Figure 8D. For larger angles, more radiation channels become available through diffraction, and the Q-matching condition is destroyed, causing emission reduction [55]. Chou *et al.* [59] proposed to fill the holes of the 2D PhC with higher index material to effectively push the diffraction threshold to 90 degrees, while maintaining a constant cutoff wavelength. Interestingly, broadband angular selectivity was theoretically and experimentally illustrated by Shen *et al.* [113], where the Brewster modes were preserved across a broadband spectrum by engineering the overlap between the band gaps of multiple 1D PhCs.

To achieve the highest possible conversion efficiencies, the view factor between the thermal emitter and the PV diode should be maximized. Hence, the emitter is usually placed in proximity to the PV diode. This arrangement often requires an efficient cooling for the PV diode to maintain high conversion efficiencies and lifetimes. Another possible strategy is to control the directionality, as well as the spectral selectivity, of the thermal emission over

the emitter's surface, so that a wide-area emitter can be placed further away from the PV diode, while maintaining a highly effective view factor. Employing surface elements, such as metallic gratings, can provide the required angular selectivity at the desired wavelengths [114]. Hence, studying thermal emitter structures with directional and spectral selectivity properties will pave the way toward this proposed thermal lensing effect.

5 PV diodes options and performance

The last step of STPV energy conversion is to convert the thermal energy radiated by thermal emitter into electricity via a PV diode. Understanding the fundamental physics and design constraints of PV diodes is very important to achieve highly efficient STPV systems.

The efficiency of a solar cell is quantified by the fraction of input power that converts to electricity and is defined as:

$$\eta_{\text{tpv}} = \frac{J_{\text{sc}} \cdot V_{\text{oc}} \cdot FF}{P_{\text{in}}} \qquad (4)$$

where P_{in} is the radiatively emitted power density from the selective emitter; J_{sc} is the short circuit current density; V_{oc} is the open circuit voltage and FF is the fill factor, defined as the quotient of the maximum power of the solar cell and the product of V_{oc} and J_{sc} [115]. A typical PV system absorbs sunlight and directly converts it into electricity by generating, dissociating and collecting electron-hole pairs at the front and back contact, respectively. Various losses may occur, reducing the performance of the PV system; among them, typically sub-band gap and thermalization losses dominate [116]. These loss mechanisms could be eliminated by employing ideal selective thermal emitter, as discussed in the preceding section.

The typical operating temperature of selective thermal emitter ranges between 1000 and 1800 K. According to Planck's blackbody spectrum and Wien's displacement law, the emission peak coincides with band gap energy E_g of PV diodes at a temperature T_B^{opt}, which is given by [7]:

$$T_B^{\text{opt}} \approx 2336[\text{K} \cdot \text{eV}^{-1}] \cdot E_g \qquad (5)$$

Unlike the optimum band gap energy (~1.3 eV) derived from the Shockley–Queisser limit in PV applications [10], the emission peak often falls in the IR region at reasonable operating temperatures. This fact indicates that PV diodes with low band gap energy (<1 eV) should be used in STPV systems to ensure good overlap between diode absorption

band edge and a selective emission spectrum. Combined with concentrated sunlight, STPV systems may exceed the Shockley–Queisser limit [28, 29, 117].

The conventional cell structure of a PV diode can be either an n-doped emitter deposited on p-doped base (n-p), or a p-doped emitter layer grown on an n-doped base layer, as illustrated in Figure 10A and 10B, depending on the favored dopant type of substrate. The front and back contacts are designed to collect positive and negative charges with low resistivity. Anti-reflection coating layers are usually placed on top of the cell to minimize reflected incident spectrum, and typically are made of SiO_2, magnesium fluoride (MgF_2) and so on. The heavily doped window layer and back surface field layers create large band offsets at the emitter and base layer to block the minority carriers from diffusing to the wrong contact and recombining with majority carriers. c-Si, Ge-based solar cells typically employ the n-p configuration since the substrate is naturally p-doped. GaSb cells usually adopt a p-n structure, with a typical tellurium-doped n-type GaSb substrate on the bottom. By employing a back contact with good reflectance to enhance photon recycling, Geisz *et al.* demonstrated a rear junction structure for III–V materials as seen in Figure 10C, which produces similar and even better performance compared with traditional structures [118].

Below, we briefly review several candidates of PV diodes in TPV applications. While indium gallium arsenide (InGaAs) has a great deal of flexibility in peak wavelengths as well as commercial success in certain applications, cost-sensitive applications may require the use of other PV technologies, such as silicon or germanium cells.

5.1 Crystalline silicon

We now consider the semiconductor materials used in the PV diode of TPV systems, including STPV. The availability of inexpensive, earth-abundant, and high-quality cells made c-Si historically the first choice for TPV and STPV applications [119, 120]. However, the band gap energy of c-Si is about 1.1 eV, which indicates that the emission peak of a blackbody emitter would never overlap with the band edge of the material, unless the emitter temperature goes above 2500 K. To date, no thermal emitter in the literature has been demonstrated to operate efficiently and sustainably at this temperature range. This mismatch between the spectral range of emission and band edge of c-Si may introduce substantial sub-band gap losses and operational inefficiencies. A silicon solar cell-based TPV system employing Yb_2O_3 thermal emitter with an efficiency of 2.4% was demonstrated by Bitnar *et al.* [120], which is far from the thermodynamic limit TPV efficiency at this band gap [117]. However, with selective emitters, recent simulation work has shown that Mo-based 2D PhCs may achieve a reasonably good efficiency of 26.2% at moderate temperatures (e.g., 1573 K) [29]. Nonetheless, despite the fact that cost-effective c-Si solar cells have been commercialized globally, they are not the best candidate to optimize the PV diode performance in TPV systems, without further improvements in selective emitter technology.

5.2 Germanium

Fabricating diodes for STPV systems with a Ge substrate is an alternative approach, since it is a relatively inexpensive material that has low-band gap energy (E_g = 0.66 eV) and excellent crystal quality in a large-size wafer [121]. Meanwhile, the low-cost fabrication process of Ge PV cells also appeal to industrial production [122]. People have reported Ge-based STPV systems with decent efficiency through different techniques [123, 124]. But in contrast with III–V materials of similar band gap energy, Ge has a relatively high density of states in the conduction band, which consequently leads to high intrinsic carrier concentration [125]. For a heavily doped (N_A~10^{17} cm^{-3}) Ge substrate, surface and bulk recombination are both high, as indicated by a low characteristic V_{OC}, compared to III–V semiconductors of similar band gap energy (e.g., GaSb) [123]. Lightly doped Ge (N_A ~2 × 10^{15} cm^{-3}) with a higher minority carrier diffusion length requires front and back passivation layers (e.g., InGaP, GaAs, α-Si) and a back mirror to reflect unabsorbed sub-band gap photons for recycling [121, 123]. However, a lightly doped Ge PV cell introduces more series resistance than a heavily doped Ge substrate. It was reported by Fraunhofer that a Ge-TPV cell illuminated by Er_2O_3 selective emission only has an efficiency of 5.34% [126]; nonetheless, its electricity cost could be competitive, given favorable assumptions of system efficiency and photocell costs [122].

5.3 Gallium antimonide

GaSb is also an option for the main PV diode of an STPV system, with its low band gap energy of 0.72 eV. Compared with Ge and c-Si, GaSb has shown a significant advantage in cell efficiency. Two processes have been introduced to fabricate GaSb PV diodes: zinc-vapor emitter diffusion and metal-organic vapor-phase epitaxial (MOVPE) growth. Under the spectrum of a W emitter at 1473 K, expected cell efficiencies for the reference current densities
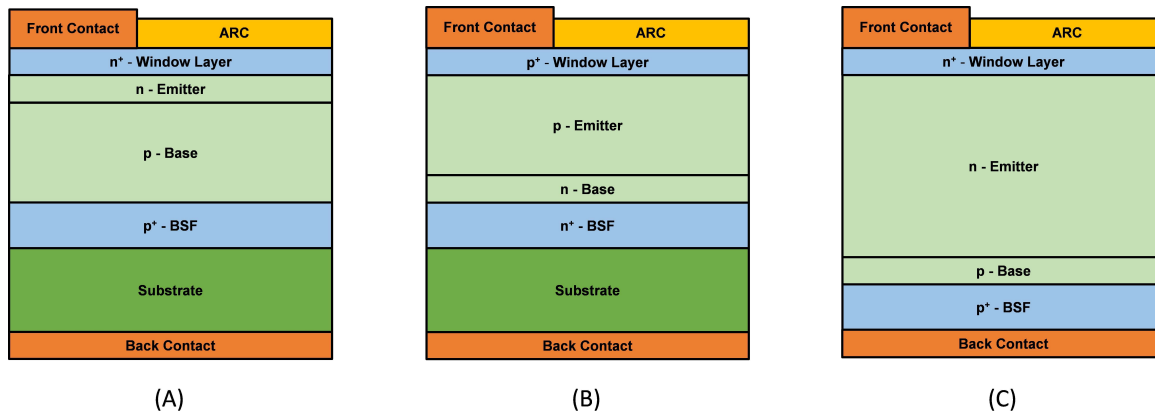
Fig. 10. Cross-sectional view of conventional cell structures of a PV diode. (A) Traditional n-type emitter on p-type base structure with p-type substrate. (B) Traditional p on n configuration with n-type substrate. (C) Thin-film III−V back-junction structure with high reflectance back contact to enhance photon recycling.

(1.5 A/cm^2) are 14.8% (zinc-diffused) and 16.6% (MOVPE), respectively [127]. Assuming 100% of sub-band gap photon recycling, calculated GaSb-based photocell efficiency could be as high as 27% for a spectral range of the W emitter between 400 and 1820 nm at 1900 K [128]. Bett and Sulima [129] also stated that efficiencies of about 30% were achievable for blackbodies at temperature $\geqslant$ 1300 K, assuming a perfect filter matched to the band edge of GaSb. However, a PV diode cannot be completely thermally isolated from the emitter in a realistic TPV system. It is expected that diode performance may degrade due to the rise of temperature. For a zinc-diffused cell, values as low as −1.4 mV/K for V_{OC} and −0.099%/K for the FF were identified between 25 and 75°C [130]. Finally, Fraas recently studied the potential fabrication costs of GaSb cells over time and reported that extrapolation to production volumes beyond 1 MW implied a substantial eventual lowering of costs [131].

5.4 Indium gallium arsenide

In$_x$Ga$_{1-x}$As is a ternary composition material whose band gap ranges from 0.4 to 1.4 eV during the epitaxial growth by varying the indium composition, allowing optimization of band gaps for various applications. It has achieved commercial acceptance in the context of quantum well laser diodes, but can have other uses, over a wide range of emission peak wavelengths. For instance, 2% of the 1473 K blackbody energy comes from photons with energy above 1.1 eV (Si) versus 15% of which above 0.72 eV (GaSb) and 35% of which above 0.55 eV InGaAs cells [132]. Indium phosphide (InP) is a popular choice for the substrate of InGaAs-based PV cell, because it both allows for epitaxial growth of low-E_g (0.55 eV) lattice-mismatched InGaAs, regular growth of lattice-matched InGaAs (0.74 eV) and maintains low absorption at the emission spectral range [133]. Although lattice-mismatched InGaAs on InP has higher defect dislocation densities, it allows 22% convertible spectrum within the radiator temperature between 1073 and 1273 K, as opposed to 12% convertible spectral energy from lattice-matched InGaAs. Recent work has shown that high-quality lattice-matched InGaAs (0.74 eV) could reach external quantum efficiency (EQE) above 90% over a wide spectral range [134]. Cost remains a big concern in InGaAs-based PV cell applications, not only because of its ternary composition, but also the sophisticated epitaxial growth recipes for the band gap of 0.55 eV. Thus, a trade-off remains between complicated epitaxial growth and the efficient use of emission spectrum over a reasonable emitter operating temperature range.

One of the major concerns of the PV diode in the STPV system is how much the emitted spectrum overlaps with the quantum efficiency spectrum of the PV diode. It is worth exploring various ternary III−V low E_g PV materials to achieve ultra-high conversion efficiencies. In the STPV system, the radiation density being incident on PV diode could be much higher than the solar irradiation intensity. Thus, it is also required that series resistance needs to be minimized, so that illuminated I−V characteristics of PV diode does not degrade severely under high radiation density [135]. Moreover, inside the STPV system, it is necessary to have an efficient cooling system to prevent degradation of the PV diode performance. Therefore, its substrate needs to be not only highly reflective to enhance photon recycling, but also be thermally conductive. Last but not least, cost-effective design of the PV diode is always one of the highest priorities in commercialization. Achieving the

best possible performance may require expensive epitaxial growth of low E_g III–V materials, such as GaSb. Thus, approaches to significantly reduce the process cost while maintaining high performance warrant detailed study.

6 Strategies for system integration

6.1 Experimental approach

An STPV system integrates multiple components. Therefore, careful engineering of the integration is as important as the optimization of each component in isolation. In this section, we will discuss three key aspects of system integration strategies: (i) the area ratio between the solar absorber and thermal emitter; (ii) the thermal management of a realistic STPV system and (iii) the measurement and calibration of both the components and the system as a whole.

In most cases, the solar absorber and the thermal emitter are assumed to be in perfect thermal contact. So in equilibrium, we have:

$$A_a[\bar{\alpha}_a(T_a)I_{solar} - \sigma\bar{\epsilon}_a(T_a)T_a^4] = A_e\sigma\bar{\epsilon}_e(T_e)T_e^4 \qquad (6)$$

$$T_a = T_e = T \qquad (7)$$

where A_a and A_e are the area of the absorber and the area of the emitter respectively; T is the temperature of the absorber/emitter; I_{solar} is the concentrated solar power incident on the selective absorber and $\bar{\epsilon}_e(T)$ is the spectrally averaged emittance of the thermal emitter. The previous equation shows that the equilibrium temperature T is dependent on both the absorber area and emitter area. In other words, T is dependent on the area ratio $\beta = \frac{A_e}{A_a}$. For a specific STPV system, there will be a β value that optimizes the efficiency under a given solar concentration [7]. This is because increasing β decreases the equilibrium temperature of the absorber/emitter structure. Lower temperature gives higher thermal transfer efficiencies, but lower STPV efficiencies. The two competing factors give rise to an optimal β. Higher solar irradiance will increase this optimal value. For a solar concentration as high as 1000 suns, β should be as large as 16 for the best performance [28].

On the system level, thermal management of the entire STPV device is critical for high performance, but oftentimes is neglected in conceptual work. Here, we discuss the thermal management necessary for each component in a STPV system.

To prevent any conduction or convection loss from the hot-side emitter to the cold-side receiver (PV diode + fil-

ter), STPV systems should be placed in a vacuum environment. Typically, a vacuum chamber providing vacuum better than 10^{-3} Torr should be sufficient [7]. The vacuum environment can also prevent oxidization of the high temperature absorber/emitter.

For high-performance STPV systems, it is preferred to have focused solar irradiance. Focusing the incident sun light, however, is not simple. The optics used to focus the solar irradiance needs to have uniform focusing effect for a broad wavelength range and endure high temperature. Recent work proposed to use an optical funnel with mirror finished inner surface to concentrate incident sunlight [7]. The geometry and dimensions of the optical funnel should match the selective solar absorber for best performance (e.g., a square solar selective absorber requires a pyramid-shape optical funnel, with an equally sized narrow square end). Nevertheless, more advanced and efficient optical concentration strategies, such as nonimaging concentrators proposed by Winston [136], could boost STPV conversion efficiencies. Furthermore, in real applications, precision tracking is important to maximize the solar concentration efficiency [63, 137].

In order to achieve high efficiency, it is also important to minimize the conductive heat loss from the solar absorber/selective emitter (at 1573 K) through its holder. This requires minimal thermal contact area, cross-sectional areas, and low thermal conductivity material(s) for the holder. However, most thermal insulating materials like high-alumina [138] are too brittle to machine when making small thermal contacts. Careful design of the absorber/emitter holder is one of the key factors required for high-performance STPV systems.

According to previous studies, the view factor from the thermal emitter to the PV diode is an important factor for both useful emission collection and the photon recycling of sub-band gap emissions. A high-performance STPV system should aim for a separation between the emitter and the PV diode of <5% of the edge length to achieve a view factor >0.9 (e.g., when the dimensions of the emitter and the PV diode are both 10 mm × 10 mm, a separation <500 μm) [139]. This requirement constrains the system design greatly. Given that the optical funnel needs to be placed in proximity to the solar absorber as well, the thickness of the absorber/ emitter holder is very limited, and can be difficult to machine. Given a narrow separation, the alignment between the absorber/emitter and the PV diode can be challenging as well. However, it has been proved that a z-axis stage is capable of maintaining a separation as small as 300 μm [7]. The challenge of the alignment can also be alleviated by adding a thermally insulating waveguide, made, for example, of dielectric PhCs, be-

tween the emitter and the PV diode. The effective view factors for both receiving useful photons and recycling sub-band gap photons can ideally approach unity, without requiring the emitter to be extremely close to the PV diode. Considering the losses due to multiple reflections within the waveguide, it would be best to minimize the use of photon recycling. Therefore, a highly selective thermal emitter should be the best fit for a waveguide-assisted STPV system.

In complete contrast with the absorber/emitter holder, the PV diode holder needs to be an excellent thermal conductor or heat sink, to cool the PV diode. One main reason for this requirement is that the PV diode power generation can be significantly impaired at high temperature. Given a finite series resistance, the short circuit current I_{sc} measured may be substantially lower than the light generated current I_l, due to the strongly temperature-dependent dark current. Therefore, it is important to control the PV diode temperature. However, for long-term operation, a small, isolated heat sink will quickly reach thermal capacity. Thus, either passive or active cooling should be added to the PV diode holder. In passive cooling strategies, an efficient thermal path needs to be created between the PV diode holder and the ambient by directly connecting the PV diode holder to the sidewalls of the vacuum chamber. Therefore, passive cooling strongly depends on the ambient temperature and the efficiency of the thermal path. On the other hand, active cooling strategies are capable of stabilizing the PV diode temperature at a certain level with better control. The most common active cooling method is cycling coolant through the PV diode holder [24, 140, 141]. Thermoelectric cooler like vacuum-compatible Peltier coolers are easier to implement, since there is no risk of coolant leakage.

6.2 Measurement and calibration

The STPV conversion efficiency can be analytically expressed as Eq. (1). Experimentally measuring the conversion efficiencies of STPV systems requires measurement of each quantity in Eq. (1) and Eq. (4). To measure I_{sc} , V_{oc} and FF, the I-V curve of the PV diode must be swept across forward biases, under illumination from the emitter. The maximum power density output can be directly derived from the I-V curve measured [6, 7], but knowing I_{sc}, V_{oc} and FF can also be helpful to analyze the PV diode performance. For concentration efficiency η_o, the concentrated solar incidence needs to be measured first. The concentrated irradiance divided by the output irradiance internally measured by the solar simulator gives η_o. It should

be carefully noted that the solar irradiance from the solar simulator needs to be calibrated according to the AM 1.5 spectrum (instead of total power density), to eliminate errors caused by the spectral deviation [142].

Understanding each step of the energy conversion is important to find out the major contribution to the efficiency loss. Therefore, it is helpful to be able to break down the system conversion efficiency into multiple steps and measure each one of them. The system conversion efficiency can be broken down as Eq. (1).

The concentration efficiency η_o can be determined using the method mentioned earlier. In contrast, direct measurement of η_t can be challenging. One way to circumvent the problem is to measure the product $\eta_t\eta_{tpv}$ first. Since $\eta_t\eta_{tpv}$ can be easily quantified by comparing the maximum power output from the PV diode with the concentrated solar power, η_{tpv} can then be quantified with an additional, direct measurement of the emitted power from the emitter. For example, a Fourier Transform Infrared (FTIR) spectrometer outside the vacuum chamber can capture the emission from the emitter through a CaF_2 window [24, 143]. With η_{tpv} quantified, η_t can then be calculated by $\frac{\eta_t\eta_{tpv}}{\eta_{tpv}}$.

6.3 Packaging for commercial deployment

STPV devices, having no fuels or chemicals to store, can be much lighter in weight and quieter during operation than traditional power generation devices. Therefore, STPV has significant potential for mobile or human-portable power production. Furthermore, a comparison with concentrated multi-junction PV systems reveals at least three potential advantages of STPV:

1. STPV involves an intermediate thermal medium, which allows for low-cost storage that improves the dispatchability of energy supply over the course of a whole day [7, 68].
2. The nonuniformity of illumination and spatial distribution of irradiance in concentrator multi-junction PV technology requires complex optical system design [144, 145]. Lattice and current matching are major challenges for multi-junction PV, which impact cost and reliability. These problems become more acute with an increasing number of junctions and novel fabrication techniques processes, such as inverted metamorphic growth [146]. By contrast, STPV systems are less sensitive to the variations in the spectral content of the concentrated illumination, and have potential to reduce

sensitivity to spatial variation through highly conductive materials.

3. The ultimate solar-to-thermal efficiency for STPV system is 85%, which closely approaches the Carnot limit [18, 27, 68, 147]. In order to achieve the ultimate thermodynamic limit of multi-junction PV efficiency, it requires the total number of junctions to be arbitrarily large.

Furthermore, when the fabrication scales up, not only the cost–effectiveness will be improved, but also the system conversion efficiency, based on prior experience in single-junction PV manufacturing [131].

Based on the comparisons listed above, it is obvious that for certain applications, STPV may be a better option. Therefore, high-performance STPV may become an important power generation strategy in the future.

However, to achieve these desirable applications, more work needs to be done regarding the packaging design, manufacturing and reliability of STPV devices. For the sake of handling and transport, it will be helpful to design the entire STPV device monolithically. This is possible because all the components of an STPV device are in solid state (except for the vacuum gap between the emitter and the PV diode) and have planar structures. The material of the packaging can be thermally insulating to isolate the high temperature absorber/emitter.

For the large-scale manufacturing, Fraas has recently pointed out that the cost of the PV diode (GaSb) circuits in TPV systems will be affordable when the volume is above 1 MW [131]. Since many STPV devices also use GaSb PV diodes, these estimates hold here as well. As for the large-scale production of selective absorbers/emitters, further research is still needed to determine the best strategy of making commercial devices that have both decent performance and affordable costs. Since the performance of an STPV device is strongly dependent on each component and the integration of the various parts, it is also important to understand its reliability physics. There are several failure mechanisms, such as vacuum leakage through the packaging, absorber/emitter structural degradation at high temperature and the PV diode degradation. The vacuum leakage may cause strong heat exchange between the emitter and the PV diode via convection and conduction, lowering the conversion efficiency and degrade the PV diode rapidly with inadequate cooling.

For nano-/microstructured selective absorber/emitters, the reliability issue also occurs at high temperatures. All-metallic nanostructures can degrade at temperatures much lower than the bulk metal melting point. Experiments have shown that nano- and microstructures degrade under high temperature exposure for long times [148–151]. Different mechanisms can lead to such degradation, including chemical reactions [33, 70, 150], recrystallization [34, 148] and surface diffusion [152, 153]. These structural degradation processes could eventually remove the fine features of the structure. This change may shift the resonance peaks, reduce the maximum emissivity [152] and thus reduce the STPV system efficiency. Fortunately, several techniques can be used to reduce the effects of these degradation mechanisms. Basically, oxidation could be greatly reduced by vacuum packaging [112, 150]. Protective layer coatings, for example, hafnium oxide (HfO$_2$) and SiO$_2$ [6, 70, 151, 154], could also greatly alleviate unwanted reactions. Moreover, using high purity, single crystalline metals [43], or pre-annealing of polycrystalline metals [150] may help in reducing recrystallization and grain growth effects. Hafnia-plugged PhCs [150] and initially curved microstructure corners [152] have been shown to be helpful in addressing surface diffusion problems. Another technique to improve thermal stability of 3D PhC structures is scaffolding metallic coatings on high-temperature materials like silicon and carbon [70, 77], while optionally utilizing high temperature dielectric adhesion layers. Figure 8E is an example of a Si scaffold with a platinum layer deposited on top (inset), as given in [70], and its spectral emissivity at high temperature. Degradation of the PV cells that may be accelerated by extreme conditions including high temperatures and humidity include corrosion, discoloration, delamination and breakage [155]. Clearly, further investigations regarding the reliability of STPV components are critical to facilitate widespread deployment of STPV.

Although the concept of STPV and its key components have been investigated for many years, full system integration and commercialization are still at an early stage. Nevertheless, making STPV practically useful in a reasonable timeframe is an important topic. Current STPV experiments require at least high vacuum. Such condition may be replaced by back-filled inert gas, but further investigation is needed to assess the increase in convective thermal losses and overall impact on reliability. A water jacket, which is a widely used PV diode cooler in current STPV experiments, may also be replaced by novel cooling strategies that are more compact and have less or zero power consumption. Together with the system packaging and reliability discussed above, these open problems are future research topics that may lead to the commercialization of STPV systems, and thus will warrant further attention.

7 Conclusions

In summary, it is clear that a broad variety of approaches can be brought to bear on the problem of STPV. Overall, an end-to-end perspective is critical to addressing the substantial remaining gap between theoretical predictions and experimental performance in STPV systems. It is clearly crucial to simultaneously design the selective thermal absorber based on the solar concentration and operating temperature available; the selective emitter based on the operating temperature and emitter band gap; and the PV absorber based on the filter and PV band gaps and operating temperature. Some of the highest-performing selective absorbers include cermets, which should be capable of up to 86% under 100 suns and 1000 K in a multilayer W/alumina cermet structure [45]. The best TPV system observed to date can give up to 23% efficiency around 1050°C, with potential for up to 50% conversion at reasonable temperatures [28]. In short, the potential space of operation is fairly large, which opens up the field to a range of approaches. Nonetheless, it is critical for those designing particular components to understand the interaction with the entirety of the system and the operating conditions to make significant progress toward higher efficiencies. Given the performance already achieved for the individual components to date, it seems clear that STPV efficiencies well over 10% should be achievable in the near term.

References

[1] Kolm HH. Solar-battery power source. Q Prog Rep, 1956, 13.

[2] Wedlock BD. Thermo-photo-voltaic conversion. Proc IEEE, 1963, 51, 694–698.

[3] Black RE, Martin L, Baldasaro PF. Thermophotovoltaics-development status and parametric considerations for power applications. Thermoelectrics, 1999. Eighteenth International Conference on, 1999, 18, 639 – 644.

[4] O'sullivan F, Celanovic I, Jovanovic N, Kassakian J, Akiyama S, Wada K. Optical characteristics of one-dimensional Si/SiO2 photonic crystals for thermophotovoltaic applications. J Appl Phys, 2005, 97, 33529.

[5] Swanson RM. A proposed thermophotovoltaic solar energy conversion system. Proc IEEE, 1979, 67, 446–447.

[6] Rinnerbauer V, Lenert A, Bierman DM, et al. Metallic photonic crystal absorber-emitter for efficient spectral control in high-temperature solar thermophotovoltaics. Adv Energy Mater, 2014, 4.

[7] Lenert A, Bierman DM, Nam Y, et al. A nanophotonic solar thermophotovoltaic device. Nat Nanotechnol, 2014, 1, 1–5.

[8] Zhang Q-C. High efficiency Al-N cermet solar coatings with double cermet layer film structures. J Phys D Appl Phys, 1999, 32, 1938–1944.

[9] Würfel P, Ruppel W. Upper limit of thermophotovoltaic solar-energy conversion. IEEE Transactions on Electron Devices, 1980, 27, 745–750.

[10] Shockley W, Queisser HJ. Detailed balance limit of efficiency of p-n junction solar cells. J Appl Phys, 1961, 32, 510–519.

[11] Demichelis F, Minetti-Mezzetti E. A solar thermophotovoltaic converter. Sol Cells, 1980, 1, 395–403.

[12] Edenburn MW. Analytical evaluation of a solar thermophotovoltaic (TPV) converter. Sol Energy, 1980, 24, 367–371.

[13] Guazzoni GE. High-temperature spectral emittance of oxides of erbium, samarium, neodymium and ytterbium. Appl Spectrosc, 1972, 26, 60–65.

[14] Höfler H, Paul HJ, Ruppel W, Würfel P. Interference filters for thermophotovoltaic solar energy conversion. Sol Cells, 1983, 10, 273–286.

[15] Ortabasi U. Rugate technology for thermophotovoltaic (TPV) applications: a new approach to near perfect filter performance. Fifth Conference on Thermophotovoltaic Generation of Electricity, 2003, 653, 249–258.

[16] Chubb DL. Reappraisal of solid selective emitters. IEEE Conf Photovolt Spec, 1990.

[17] Spirkl W, Ries H. Solar thermophotovoltaics: An assessment. J Appl Phys, 1985, 57, 4409–4414.

[18] Harder N-P, Würfel P. Theoretical limits of thermophotovoltaic solar energy conversion. Semicond Sci Technol, 2003, 18, S151–S157.

[19] Bett AW, Keser S, Stollwerck G, Sulima O V, Wettling W. GaSb-based (thermo)photovoltaic cells with Zn diffused emitters. Conf Rec Twenty Fifth IEEE Photovolt Spec Conf 1996, 1996.

[20] Fraas LM, Girard GR, Avery JE, et al. GaSb booster cells for over 30% efficient solar-cell stacks. J Appl Phys, 1989, 66, 3866.

[21] Stone KW, Leingang EF, Kusek SMM, Drubka REE, Fay TDD. On-Sun test results of McDonnell Douglas' prototype solar thermophotovoltaic power system. Proceedings of 1994 IEEE 1st World Conference on Photovoltaic Energy Conversion - WCPEC (A Joint Conference of PVSC, PVSEC and PSEC), 1994, 2, 2010–2013.

[22] Stone KW, Fatemi NS, Garverick LM. Operation and component testing of a solar thermophotovoltaic power system. Conf Rec Twenty Fifth IEEE Photovolt Spec Conf - 1996, 1996, 1421–1424.

[23] Wanlass MW. Recent advances in low-bandgap, InP-based GaInAs/InAsP materials and devices for thermophotovoltaic (TPV) energy conversion. AIP Conf Proc, 2004, 738, 427–435.

[24] Yugami H, Sai H, Nakamura K, Nakagawa N, Ohtsubo H. Solar thermophotovoltaic using Al2O3 / Er3/Al5/O12 eutectic

composite selective emitter. Conf Rec Twenty-Eighth IEEE Photovolt Spec Conf 2000, 2000, 1, 1214–1217.

[25] Datas A, Algora C, Zamorano JC, et al. A solar TPV system based on germanium cells. AIP Conference Proceedings, 2007, 890, 280–290.

[26] Ungaro C, Gray SK, Gupta MC. Solar thermophotovoltaic system using nanostructures. Opt Express, 2015, 23, A1149.

[27] Harder N-P, Green MA. Thermophotonics. Semicond Sci Technol, 2003, 18, S270.

[28] Rephaeli E, Fan S. Absorber and emitter for solar thermophotovoltaic systems to achieve efficiency exceeding the Shockley-Queisser limit. Opt Express, 2009, 17, 15145–59.

[29] Zhou Z, Chen Q, Bermel P. Prospects for high-performance thermophotovoltaic conversion efficiencies exceeding the Shockley–Queisser limit. Energy Convers Manag, 2015, 97, 63–69.

[30] Kennedy C. Review of mid-to high-temperature solar selective absorber materials. NREL Tech Rep, 2002, 1617, 1–58.

[31] Sathiaraj TS, Thangarj R, Sharbaty AA, Bhatnagar M, Agnihotri OP. Ni-Al2O3 selective cermet coatings for photochemical conversion up to 500 C. Thin Solid Films, 1990, 190, 241.

[32] Sergeant NP, Pincon O, Agrawal M, Peumans P. Design of wide-angle solar-selective absorbers using aperiodic metal-dielectric stacks. Opt Express, 2009, 17, 22800–22812.

[33] Rinnerbauer V, Yeng YX, Chan WR, et al. High-temperature stability and selective thermal emission of polycrystalline tantalum photonic crystals. Opt Express, 2013, 21, 11482–91.

[34] Sai H, Kanamori Y, Yugami H. High-temperature resistive surface grating for spectral control of thermal radiation. Appl Phys Lett, 2003, 82, 1685.

[35] Cuomo JJ, Ziegler JF, Woodall JM. A new concept for solar energy thermal conversion. Appl Phys Lett, 1975, 26, 557–559.

[36] Pellegrini G. Experimental methods for the preparation of selectively absorbing textured surfaces for photothermal solar conversion. Sol energy Mater, 1980, 3, 391–404.

[37] Lehmann HW. Profile control by reactive sputter etching. J Vac Sci Technol, 1978, 15, 319.

[38] Seraphin BO. Optical properties of solids: new developments. North Holland Publishing Co., Amsterdam, 1976.

[39] Randich E, Allred DD. Chemically vapor-deposited ZrB2 as a selective solar absorber. Thin Solid Films, 1981, 83, 393–398.

[40] Agnihotri OP, Gupta BK. Solar selective surfaces. New York: Wiley-Interscience Pub, 1981.

[41] Zhang Q, Mills DR. Very low-emittance solar selective surfaces using new film structures. J Appl Phys, 2006, 72, 3013–3021.

[42] Gao P, Meng LJ, Dos Santos MP, Teixeira V, Andritschky M. Study of ZrO2-Y2O3 films prepared by rf magnetron reactive sputtering. Thin Solid Films, 2000, 377–378, 32–36.

[43] Arancibia-Bulnes CA, Estrada CA, Ruiz-Suárez JC. Solar absorptance and thermal emittance of cermets with large particles. J Phys D Appl Phys, 2000, 33, 2489–2496.

[44] Niklasson GA, Granqvist CG. Selectively solar-absorbing surface coatings: optical properties and degradation. Materials science for solar energy conversion systems, Pergamon, Oxford, UK, 1991.

[45] Chester D, Bermel P, Joannopoulos JD, Soljacic M, Celanovic I. Design and global optimization of high-efficiency solar

[46] Messier R, Krishnaswamy S V., Gilbert LR, Swab P. Black a-Si solar selective absorber surfaces. J Appl Phys, 1980, 51, 1611.

[47] Seraphin BO. Chemical vapor deposition of thin semiconductor films for solar energy conversion. Thin Solid Films, 1976, 39, 87–94.

[48] Gilbert LR, Messier R, Roy R. Black germanium solar selective absorber surfaces. Thin Solid Films, 1978, 54, 149–157.

[49] Mattox DM. Deposition of semiconductor films with high solar absorptivity. J Vac Sci Technol, 1975, 12, 182.

[50] Bermel P, Ghebrebrhan M, Chan W, et al. Design and global optimization of high-efficiency thermophotovoltaic systems. Opt Express, 2010, 18, A314–A334.

[51] Wang X, Li H, Yu X, Shi X, Liu J. High-performance solution-processed plasmonic Ni nanochain-Al 2O3 selective solar thermal absorbers. Appl Phys Lett, 2012, 101, 1–6.

[52] Wu C, Neuner III B, John J, et al. Metamaterial-based integrated plasmonic absorber/emitter for solar thermophotovoltaic systems. J Opt, 2012, 14, 024005.

[53] Guler U, Boltasseva A, Shalaev VM. Refractory plasmonics. Science (80), 2014, 344, 263–264.

[54] Liu J, Guler U, Li W, Kildishev A, Boltasseva A, Shalaev VM. High-temperature plasmonic thermal emitter for thermophotovotaics. CLEO, 2014, 1, FM4C.5.

[55] Yeng YX, Ghebrebrhan M, Bermel P, et al. Enabling high-temperature nanophotonics for energy applications. Proc Natl Acad Sci U S A, 2012, 109, 2280–5.

[56] Ghebrebrhan M, Bermel P, Yeng YX, Celanovic I, Soljačić M, Joannopoulos JD. Tailoring thermal emission via Q matching of photonic crystal resonances. Phys Rev A, 2011, 83, 033810.

[57] Joannopoulos JD, Johnson SG, Winn JN, Meade RD. Photonic crystals molding the flow of light. Second. Princeton, NJ: Princeton University Press, 2008.

[58] Sergeant NP, Agrawal M, Peumans P. High performance solar-selective absorbers using coated sub-wavelength gratings. Opt Express, 2010, 18, 5525–5540.

[59] Chou JB, Yeng YX, Lenert A, et al. Design of wide-angle selective absorbers/emitters with dielectric filled metallic photonic crystals for energy applications. Opt Express, 2014, 22, A144–54.

[60] Sai H, Yugami H, Kanamori Y, Hane K. Solar selective absorbers based on two-dimensional W surface gratings with submicron periods for high-temperature photothermal conversion. Sol Energy Mater Sol Cells, 2003, 79, 35–49.

[61] Fleming JG, Lin SY, El-Kady I, Biswas R, Ho KM. All-metallic three-dimensional photonic crystals with a large infrared bandgap. Nature, 2002, 417, 52–5.

[62] Rinnerbauer VR, Ausecker EL, Chäffler FS, Eininger PR, Trasser GS, Eil RDG. Nanoimprinted superlattice metallic photonic crystal as ultraselective solar absorber. 2015, 2, 18–21.

[63] Mousazadeh H, Keyhani A, Javadi A, Mobli H, Abrinia K, Sharifi A. A review of principle and sun-tracking methods for maximizing solar systems output. Renew Sustain Energy Rev, 2009, 13, 1800–1818.

[64] Chubb D, Pal A, Patton M, Jenkins P. Rare earth doped high temperature ceramic selective emitters. J Eur Ceram Soc, 1999, 19, 2551–2562.

[65] Bitnar B, Durisch W, Mayor J-C, Sigg H, Tschudi HR. Characterisation of rare earth selective emitters for thermophotovoltaic applications. Sol Energy Mater Sol Cells, 2002, 73, 221–234.

[66] Torsello G, Lomascolo M, Licciulli A, Diso D, Tundo S, Mazzer M. The origin of highly efficient selective emission in rare-earth oxides for thermophotovoltaic applications. Nat Mater, 2004, 3, 632–7.

[67] Bitnar B, Durisch W, Holzner R. Thermophotovoltaics on the move to applications. Appl Energy, 2013, 105, 430–438.

[68] Nam Y, Yeng YX, Lenert A, et al. Solar thermophotovoltaic energy conversion systems with two-dimensional tantalum photonic crystal absorbers and emitters. Sol Energy Mater Sol Cells, 2014, 122, 287–296.

[69] Celanovic I, Jovanovic N, Kassakian J. Two-dimensional tungsten photonic crystals as selective thermal emitters. Appl Phys Lett, 2008, 92, 193101.

[70] Garín M, Hernández D, Trifonov T, Alcubilla R. Three-dimensional metallo-dielectric selective thermal emitters with high-temperature stability for thermophotovoltaic applications. Sol Energy Mater Sol Cells, 2015, 134, 22–28.

[71] Liu X, Tyler T, Starr T, Starr AF, Jokerst NM, Padilla WJ. Taming the blackbody with infrared metamaterials as selective thermal emitters. Phys Rev Lett, 2011, 107, 045901.

[72] Tobler WJ, Durisch W. Plasma-spray coated rare-earth oxides on molybdenum disilicide – High temperature stable emitters for thermophotovoltaics. Appl Energy, 2008, 85, 371–383.

[73] Khan MR, Wang X, Sakr E, Alam MA, Bermel P. Enhanced selective thermal emission with a meta-mirror following Generalized Snell's Law. MRS Proceedings, 2015, 1728.

[74] Sakr ES, Zhou Z, Bermel P. High efficiency rare-earth emitter for thermophotovoltaic applications. Appl Phys Lett, 2014, 105, 111107.

[75] Kohiyama A, Shimizu M, Kobayashi H, Iguchi F, Yugami H. Spectrally controlled thermal radiation based on surface microstructures for high-efficiency solar thermophotovoltaic system. Energy Procedia, 2014, 57, 517–523.

[76] Lee J-H, Kim Y-S, Constant K, Ho K-M. Woodpile metallic photonic crystals fabricated by using soft lithography for tailored thermal emission. Adv Mater, 2007, 19, 791–794.

[77] Nagpal P, Josephson DP, Denny NR, DeWilde J, Norris DJ, Stein A. Fabrication of carbon/refractory metal nanocomposites as thermally stable metallic photonic crystals. J Mater Chem, 2011, 21, 10836.

[78] Qi M, Lidorikis E, Rakich PT, et al. A three-dimensional optical photonic crystal with designed point defects. Nature, 2004, 429, 538–42.

[79] Rybicki GB, Lightman AP. Radiative processes in astrophysics. Weinheim, Germany: Wiley-VCH Verlag GmbH, 1985.

[80] Rytov SM, Kravtsov YA, Tatarskii VI. Principles of statistical radiophysics. New York: Springer-Verlag, 1987.

[81] Basu S, Zhang ZM, Fu CJ. Review of near-field thermal radiation and its application to energy conversion. Int J Energy Res, 2009, 33, 1203–1232.

[82] Molesky S, Jacob Z. Ideal near-field thermophotovoltaic cells. Phys Rev B, 2015, 91, 205435.

[83] Francoeur M, Vaillon R, Menguc MP. Performance analysis of nanoscale-gap thermophotovoltaic energy conversion devices. ICHMT Digit Libr ONLINE, 2011.

[84] Bernardi MP, Dupré O, Blandre E, Chapuis P-O, Vaillon R, Francoeur M. Impacts of propagating, frustrated and surface modes on radiative, electrical and thermal losses in nanoscale-gap thermophotovoltaic power generators. Sci Rep, 2015, 5, 11626.

[85] Ben-Abdallah P, Marquier F, Greffet J-J. Controlling thermal radiation with surface waves. Plasmonics: theory and applications, T. V. Shahbazyan and M. I. Stockman, Eds. New York: Springer Science & Business Media, 2014, 592.

[86] Celanovic I, Perreault D, Kassakian J. Resonant-cavity enhanced thermal emission. Phys Rev B, 2005, 72, 075127.

[87] Rinnerbauer V, Ndao S, Xiang Yeng Y, et al. Large-area fabrication of high aspect ratio tantalum photonic crystals for high-temperature selective emitters. J Vac Sci Technol B Microelectron Nanom Struct, 2013, 31, 011802.

[88] Zenker M, Heinzel A, Stollwerck G, Ferber J, Luther J. Efficiency and power density potential of combustion-driven thermophotovoltaic systems using GaSb photovoltaic cells. IEEE Trans Electron Devices, 2001, 48, 367–376.

[89] Vigil O, Ruiz CM, Seuret D, Bermúdez V, Diéguez E. Transparent conducting oxides as selective filters in thermophotovoltaic devices. J Phys Condens Matter, 2005, 17, 6377–6384.

[90] Qian ZG, Shen WZ, Ogawa H, Guo QX. Infrared reflection characteristics in InN thin films grown by magnetron sputtering for the application of plasma filters. J Appl Phys, 2002, 92, 3683.

[91] Mao L, Ye H. New development of one-dimensional Si/SiO2 photonic crystals filter for thermophotovoltaic applications. Renew Energy, 2010, 35, 249–256.

[92] Mostafa SI, Rafat NH, El-Naggar SA. One-dimensional metallic-dielectric (Ag/SiO2) photonic crystals filter for thermophotovoltaic applications. Renew Energy, 2012, 45, 245–250.

[93] Bovard BG. Rugate filter theory: an overview. Appl Opt, 1993, 32, 5427–42.

[94] Carniglia CK. Comparison of several shortwave pass filter designs. Appl Opt, 1989, 28, 2820–3.

[95] Ganapati V. Optical design considerations for high conversion efficiency in photovoltaics. University of California, Berkeley, 2015.

[96] Laroche M, Carminati R, Greffet J-J. Near-field thermophotovoltaic energy conversion. J Appl Phys, 2006.

[97] Ilic O, Jablan M, Joannopoulos JD, Celanovic I, Soljačić M. Overcoming the black body limit in plasmonic and graphene near-field thermophotovoltaic systems. Optics Express, 2012, 20. A366.

[98] Narayanaswamy A, Chen G. Surface modes for near field thermophotovoltaics. Appl Phys Lett, 2003.

[99] Domoto GA, Boehm RF, Tien CL. Experimental investigation of radiative transfer between metallic surfaces at cryogenic temperatures. J Heat Transfer, 1970, 92, 412.

[100] Hargreaves C. Anomalous radiative transfer between closely-spaced bodies. Phys Lett A, 1969, 30, 491–492.

[101] Polder D, van Hove M. Theory of radiative heat transfer between closely spaced bodies. Phys Rev B, 1971, 4, 3303–3314.

[102] Volokitin AI, Persson BNJ. Near-field radiative heat transfer and noncontact friction. Rev Mod Phys, 2007, 79, 1291–1329.

[103] Joulain K, Mulet J-P, Marquier F, Carminati R, Greffet J-J. Surface electromagnetic waves thermally excited: Radiative heat

transfer, coherence properties and Casimir forces revisited in the near field. Surf Sci Rep, 2005, 57, 59–112.

[104] DiMatteo RS, Greiff P, Finberg SL, et al. Enhanced photogeneration of carriers in a semiconductor via coupling across a nonisothermal nanoscale vacuum gap. Appl Phys Lett, 2001, 79, 1894.

[105] DiMatteo R, Greiff P, Finberg S, et al. Micron-gap ThermoPhotoVoltaics (MTPV). Proc 6th Conf Thermophotovoltaic Gener Electr, 2004, 738, 42–51.

[106] Hanamura K, Mori K. Nano-gap TPV generation of electricity through evanescent wave in near-field above emitter surface. AIP Conference Proceedings, 2007.

[107] Messina R, Ben-Abdallah P. Graphene-based photovoltaic cells for near-field thermal energy conversion. Sci Rep, 2013.

[108] Park K, Basu S, King WP, Zhang ZM. Performance analysis of near-field thermophotovoltaic devices considering absorption distribution. 2008, 109, 305–316.

[109] Francoeur M, Vaillon R, Mengüç MP. Thermal impacts on the performance of nanoscale-gap thermophotovoltaic power generators. IEEE Trans Energy Convers, 2011.

[110] Tong JK, Hsu W-C, Huang Y, Boriskina S V, Chen G. Thin-film 'thermal well' emitters and absorbers for high efficiency thermophotovoltaics. Sci Rep, 2015.

[111] Guo Y, Jacob Z. Thermal hyperbolic metamaterials. Opt Express, 2013, 21, 15014–9.

[112] Bauer T. Thermophotovoltaics: basic principles and critical aspects of system design. Berlin: Springer, 2011.

[113] Shen Y, Ye D, Celanovic I, Johnson SG, Joannopoulos JD, Soljačić M. Optical broadband angular selectivity. Science, 2014, 343, 1499–501.

[114] Laroche M, Arnold C, Marquier F, et al. Highly directional radiation generated by a tungsten thermal source. Opt Lett, 2005, 30, 2623.

[115] Bermel P, Chan W, Yeng YX, Joannopoulos JD, Soljacic M, Celanovic I. Design and global optimization of high-efficiency thermophotovoltaic systems. TPV9: Ninth World Conference on Thermophotovoltaic Generation of Electricity, 2010.

[116] Hirst LC, Ekins-Daukes NJ. Fundamental losses in solar cells. Prog Photovoltaics Res Appl, 2011, 19, 286–293.

[117] Baldasaro PF, Raynolds JE, Charache GW, et al. Thermodynamic analysis of thermophotovoltaic efficiency and power density tradeoffs. J Appl Phys, 2001, 89, 3319–3327.

[118] Geisz JF, Steiner MA, García I, Kurtz SR, Friedman DJ. Enhanced external radiative efficiency for 20.8% efficient single-junction GaInP solar cells. Appl. Phys. Lett., 2013, 103, 2011–2016.

[119] Bitnar B. Silicon, germanium and silicon/germanium photocells for thermophotovoltaics applications. Semicond Sci Technol, 2003, 18, S221–S227.

[120] Bitnar B, Durisch W, Grutzmacher D, et al. A TPV system with silicon photocells and a selective emitter. Conf Rec Twenty-Eighth IEEE Photovolt Spec Conf - 2000 (Cat No00CH37036), 2000, 1218–1221.

[121] Fernandez J, Dimroth F, Oliva E, Hermle M, Bett AW. Backsurface optimization of germanium TPV cells. AIP Conference Proceedings 890; TPV7: Seventh World Conference on Thermophotovoltaic Generation of Electricity, 2007, 890, 190–197.

[122] van der Heide J, Posthuma NE, Flamand G, Poortmans J. Development of low-cost thermophotovoltaic cells using germanium substrates. AIP Conf Proc, 2007, 890, 129–138.

[123] Khvostikov VP, Khvostikova OA, Gazaryan PY, et al. Photoconverters for solar TPV systems. Conference Record of the 2006 IEEE 4th World Conference on Photovoltaic Energy Conversion, WCPEC-4, 2007, 1, 667–670.

[124] Nagashima T, Hokoi K, Okumura K, Yamaguchi M. Surface passivation for germanium and silicon back contact type photovoltaic cells. In Photovoltaic Energy Conversion, Conference Record of the 2006 IEEE 4th World Conference on 2006 1, 655–658.

[125] Tan M, Ji L, Wu Y, et al. Investigation of InGaAs thermophotovoltaic cells under blackbody radiation. Appl Phys Express, 2014, 7, 096601.

[126] van der Heide J, Posthuma NE, Flamand G, Geens W, Poortmans J. Cost-efficient thermophotovoltaic cells based on germanium substrates. Sol Energy Mater Sol Cells, 2009, 93, 1810–1816.

[127] Schlegl T, Dimroth F, Ohm A, Bett AW. TPV modules based on GaSb structures. AIP Conf Proc 738; TPV6 Sixth World Conf Thermophotovoltaic Gener Electr, 2004, 738, 285–293.

[128] Andreev VM, Sorokina SV, Timoshina NK, Khvostikov VP, Shvarts MZ. Solar cells based on gallium antimonide. Semiconductors, 2009, 43, 668–671.

[129] Bett AW, Sulima OV. GaSb photovoltaic cells for applications in TPV generators. Semicond Sci Technol, 2003, 18, S184–S190.

[130] Sulima OV, Bett AW. Fabrication and simulation of GaSb thermophotovoltaic cells. Sol Energy Mater Sol Cells, 2001, 66, 533–540.

[131] Fraas LM. Low-cost solar electric power. Springer Cham Heidelberg New York Dordrecht London, 2014.

[132] Wojtczuk S. Low bandgap InGaAs thermophotovoltaic cells. IECEC 96 Proc 31st Intersoc Energy Convers Eng Conf, 1996, 2, 1–5.

[133] Murray SL, Newman FD, Murray CS, et al. MOCVD growth of lattice-matched and mismatched InGaAs materials for thermophotovoltaic energy conversion. Semicond Sci Technol, 2003, 18, S202–S208.

[134] Tuley RS, Orr JMS, Nicholas RJ, Rogers DC, Cannard PJ, Dosanjh S. Lattice-matched InGaAs on InP thermophovoltaic cells. Semicond Sci Technol, 2013, 28, 015013.

[135] Daneshvar H, Prinja R, Kherani NP. Thermophotovoltaics: Fundamentals, challenges and prospects. Appl Energy, 2015, 159, 560–575.

[136] Winston R. Thermodynamically efficient solar concentrators. J Photonics Energy, 2012, 2, 25501–25506.

[137] Kim YS, Kang SM, Winston R. Tracking control of high-concentration photovoltaic systems for minimizing power losses. Progress in Photovoltaics: Research and Applications, 20, 6–11, 2012.

[138] Munz D, Fett T. Ceramics: mechanical properties, failure behaviour, materials selection. 1999.

[139] Incropera FP, DeWitt DP. Fundamentals of heat transfer. New York: John Wiley and Sons, 1981.

[140] Fraas L, Samaras J, Avery J, Minkin L. Antireflection coated refractory metal matched emitters for use with GaSb thermophotovoltaic generators. Conf Rec Twenty-Eighth IEEE Photovolt Spec Conf - 2000, 2000, 1020–1023.

[141] Andreev VM, Khvostikov VP, Khvostikova OA, et al. Solar thermophotovoltaic system with high temperature tungsten emitter. Conf Rec Thirty-first IEEE Photovolt Spec Conf 2005, 2005.

[142] Kasten F, Young AT. Revised optical air mass tables and approximation formula. Appl Opt, 1989, 28, 4735–4738.

[143] Yu Z, Sergeant NP, Skauli T, Zhang G, Wang H, Fan S. Enhancing far-field thermal emission with thermal extraction. Nat Commun, 2013, 4, 1730.

[144] Herrero R, Victoria M, Domínguez C, Askins S, Antón I, Sala G. Concentration photovoltaic optical system irradiance distribution measurements and its effect on multi-junction solar cells. Prog Photovoltaics Res Appl, 2012, 20, 6–11.

[145] Victoria M, Herrero R, Domínguez C, Antón I, Askins S, Sala G. Characterization of the spatial distribution of irradiance and spectrum in concentrating photovoltaic systems and their effect on multi-junction solar cells. Prog Photovoltaics Res Appl, 2013, 21, 308–318.

[146] Jones RK, Ermer JH, Fetzer CM, King RR. Evolution of multijunction solar cell technology for concentrating photovoltaics. Japanese J Applied Phys, 2012, 51, 1–4.

[147] Datas A, Algora C. Global optimization of solar thermophotovoltaic systems. Prog Photovoltaics Res Appl, 2013, 21, 1040–1055.

[148] Schlemmer C. Thermal stability of micro-structured selective tungsten emitters. AIP Conference Proceedings, 2003, 653, 164–173.

[149] Denny NR, Li F, Norris DJ, Stein A. In situ high temperature TEM analysis of sintering in nanostructured tungsten and tungsten–molybdenum alloy photonic crystals. J Mater Chem, 2010, 20, 1538–1545.

[150] Lee H-J, Smyth K, Bathurst S, et al. Hafnia-plugged microcavities for thermal stability of selective emitters. Appl Phys Lett, 2013, 102, 241904.

[151] Arpin KA, Losego MD, Braun P V. Electrodeposited 3D tungsten photonic crystals with enhanced thermal stability. Chem Mater, 2011, 23, 4783–4788.

[152] Peykov D, Yeng YX, Celanovic I, Joannopoulos JD, Schuh CA. Effects of surface diffusion on high temperature selective emitters. Opt Express, 2015, 23, 9979–93.

[153] Mullins WW. Flattening of a nearly plane solid surface due to capillarity. J Appl Phys, 1959, 30, 77.

[154] Arpin KA, Losego MD, Cloud AN, et al. Three-dimensional self-assembled photonic crystals with high temperature stability for thermal emission modification. Nat Commun, 2013, 4, 2630.

[155] Ndiaye A, Charki A, Kobi A, Kébé CMF, Ndiaye PA, Sambou V. Degradations of silicon photovoltaic modules: A literature review. Sol Energy, 2013, 96, 140–151.